Combustion Noise

Dowling, A. P., & Mahmoudi, Y. (2015). Combustion Noise. *Proceedings of the Combustion Institute*, *35*(1), 65-100. https://doi.org/10.1016/j.proci.2014.08.016

Published in:
Proceedings of the Combustion Institute

Document Version:
Publisher's PDF, also known as Version of record

Queen's University Belfast - Research Portal:
Link to publication record in Queen's University Belfast Research Portal

Available online at www.sciencedirect.com

ScienceDirect

Proceedings of the Combustion Institute 35 (2015) 65–100

Proceedings of the Combustion Institute

www.elsevier.com/locate/proci

Combustion noise

Ann P. Dowling *, Yasser Mahmoudi

Department of Engineering, University of Cambridge, Cambridge CB2 1PZ, United Kingdom

Available online 22 November 2014

Abstract

Combustion noise is becoming increasingly important as a major noise source in aeroengines and ground based gas turbines. This is partially because advances in design have reduced the other noise sources, and partially because next generation combustion modes burn more unsteadily, resulting in increased external noise from the combustion. This review reports recent progress made in understanding combustion noise by theoretical, numerical and experimental investigations. We first discuss the fundamentals of the sound emission from a combustion region. Then the noise of open turbulent flames is summarized. We subsequently address the effects of confinement on combustion noise. In this case not only is the sound generated by the combustion influenced by its transmission through the boundaries of the combustion chamber, there is also the possibility of a significant additional source, the so-called 'indirect' combustion noise. This involves hot spots (entropy fluctuations) or vorticity perturbations produced by temporal variations in combustion, which generate pressure waves (sound) as they accelerate through any restriction at the exit of the combustor. We describe the general characteristics of direct and indirect noise. To gain further insight into the physical phenomena of direct and indirect sound, we investigate a simple configuration consisting of a cylindrical or annular combustor with a low Mach number flow in which a flame zone burns unsteadily. Using a low Mach number approximation, algebraic exact solutions are developed so that the parameters controlling the generation of acoustic, entropic and vortical waves can be investigated. The validity of the low Mach number approximation is then verified by solving the linearized Euler equations numerically for a wide range of inlet Mach numbers, stagnation temperature ratios, frequency and mode number of heat release fluctuations. The effects of these parameters on the magnitude of the waves produced by the unsteady combustion are investigated. In particular the magnitude of the indirect and direct noise generated in a model combustor with a choked outlet is analyzed for a wide range of frequencies, inlet Mach numbers and stagnation temperature ratios. Finally, we summarize some of the unsolved questions that need to be the focus of future research.

Keywords: Combustion noise; Acoustic perturbation; Entropy perturbation; Vorticity perturbation; Choked nozzle

1. Introduction

In the last four decades noise emission has developed into a topic of increasing concern to society. This mainly stems from the adverse physiological impacts on those exposed to noise over

* Corresponding author.
E-mail address: apd1@cam.ac.uk (A.P. Dowling).

http://dx.doi.org/10.1016/j.proci.2014.08.016

lengthy periods. As a result, in air, road and rail transport technologies, the control of noise emissions is central to social acceptance and economic competitiveness. Due to its intermittent nature, aircraft noise is deemed to be the most annoying transportation noise, with road noise being the least likely to annoy. Noise has an immediate effect upon observers at the time of emission, causing annoyance and physiological change, and it also impedes the efficiency of observers. Longer term effects of noise are physiological impairment, e.g. hearing damage, speech and sleep interference. Although individual aircraft have become less noisy over the last 30 years, the increase in air traffic means that many citizens are concerned by aircraft noise. According to the International Civil Aviation Organization [1], global air transportation is anticipated to double over the next couple of decades. It is therefore expected that the negative social and environmental impacts of its noise emission will increase.

Aircraft noise is noise pollution produced by any aircraft or its components during various phases of a flight: on the ground such as auxiliary power units, while taxiing, on run-up, during take-off, underneath and lateral to departure and arrival paths, or during landing. The primary source of noise in an aircraft can be contributed to the fan, compressor, combustor, turbine, and jet exhaust [2] (see Fig. 1). On approach the airframe is also a significant source of noise.

During the last few decades, research efforts have enabled a significant reduction of jet, fan and external aerodynamic noise. The reduction of jet noise was mainly achieved by introducing ultra-high-bypass ratio turbofan engines. Fan noise has been reduced through effective acoustic liners and complex designs of fan blade geometry. These efforts on the reduction of jet and fan noise have left combustion noise as an important remaining contributor [2,3]. Figure 2 shows the significance of combustion noise relative to other noise sources for a typical turbojet application.

Combustion noise appears to be the third dominant source in the whole turbojet engine noise after fan and jet noise, especially at approach and cut back conditions. Furthermore, recent studies on low-NOx combustors such as lean premixed prevaporized (LPP) combustion show considerable increase in noise emission [4]. This is because lean premixed and stratified combustion burns more unsteadily [5–7]. As discussed in these references, lean premixed combustors can also be susceptible to an instability arising from the feedback interaction between unsteady combustion and acoustic waves. Such an instability occurs at a discrete tone related to the acoustic resonances of the combustor usually shifted slightly by the flame response. Even when the self-excited instability has been eliminated by a careful combustor design, which reduces the sensitivity of the rate of combustion to acoustic waves, LPP systems generate substantial broad-band noise, which can be heard outside the engine. Furthermore, noise from auxiliary power units (APU) is an important contributor to the overall level of ramp noise (the noise generated by an aircraft while it is on the ground, typically parked at the ramp). A significant component of APU noise is combustion noise [8,9]. It is therefore crucial to investigate this broad-band combustion noise and develop methods to predict and reduce it, in order to enable the introduction of low noise, green technologies on next generation low-NOx combustors and premixed burners in aero-engines [7,10,11].

2. Motivation: Gas turbine combustion noise sources

The total noise radiated by a gas turbine combustion chamber system consists of direct and indirect combustion noise [11,12]. The direct noise sources are related to the unsteady processes of volumetric expansion and contraction in the reactive region [13,14]. This is generated by the fluctuation of heat release rate associated with the chemical reaction [11,15]. It would occur even if the combustion were in unbounded space, although in the gas turbine the sound radiated is modified from the open flame result by its transmission from the combustion chamber to the far-field through the turbine and jet. The indirect combustion noise, identified by the early works of Marble and Candel [12] and Morfey [16] in the seventies, is an additional noise generated when a fluid with a non-uniform entropy or vorticity distribution is accelerated, as it is when convected through the choked nozzle located at the outlet of the combustion chamber in a gas turbine [17,18]. A summary of these different core noise sources is illustrated in Fig. 3.

The spatial and temporal variation of the rate of combustion produces hot and cold spots which are convected by the mean flow [11]. The coupling between hot spots generated by combustion and particle acceleration in the mean flow then gives rise to pressure perturbations. Since the entropy of the hot spots is different to that of the surrounding, indirect noise is also called entropy noise. The vital role of acceleration/deceleration caused Ffowcs Williams and Howe [17] to refer to it as acoustical *bremsstrahlung*. The combustion also generates unsteady shear leading to vorticity perturbations [19], which also convect and generate pressure perturbations as they accelerate through the turbine nozzle guide vanes. Hence, at the combustor exit the interaction of the vortical and entropic perturbations with the mean streamwise velocity gradient results in energy transfer to an acoustic mode [19,20]. Acceleration of entropy and vorticity waves in the choked

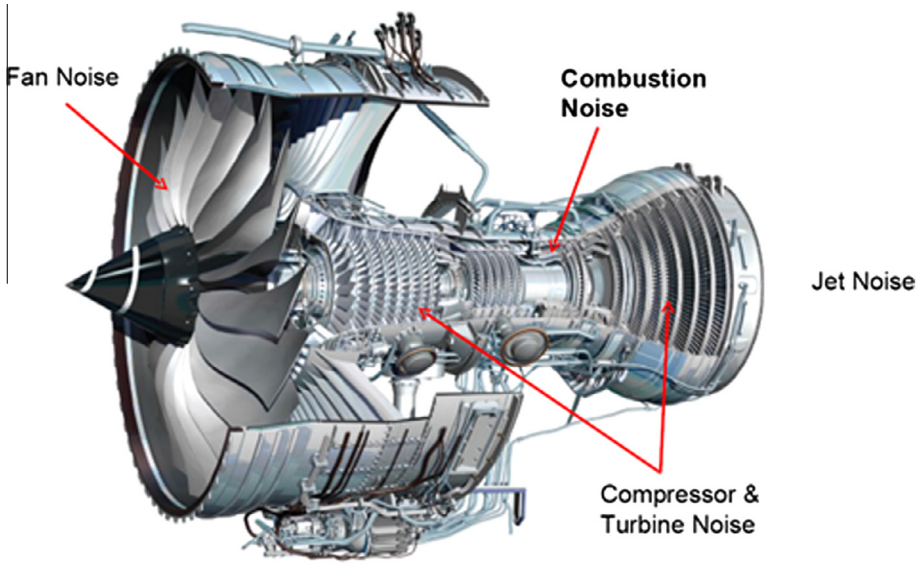

Fig. 1. Summary of engine noise sources (Rolls-Royce Trent 1000, copyright Rolls-Royce, published with permission).

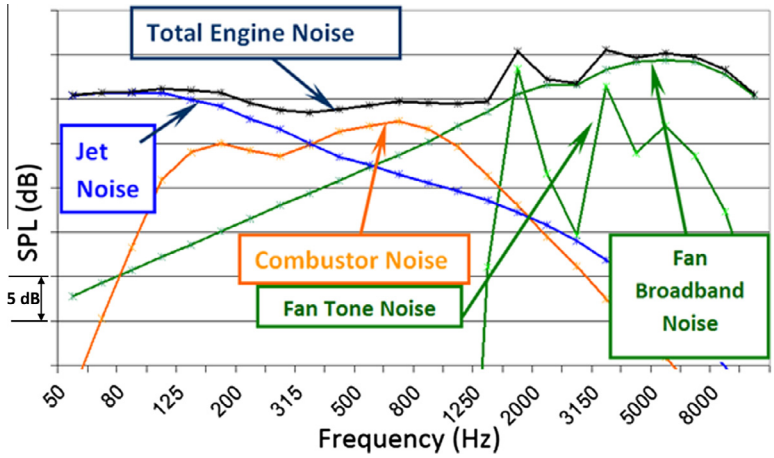

Fig. 2. Typical contribution of noise sources on a turbojet engine at approach. (Fig. 2 is from SAFRAN Snecma (http://www.safran-group.com/), published with permission).

nozzle results in generation of pressure waves that propagate upstream (from where they can be reflected from the flame zone and/or the upstream geometry altering the downstream propagating waves) and downstream from the turbine stage as indirect combustion noise [12,17,18].

In this review we discuss combustion noise arising from fluctuations in the rate of heat release in a turbulent flame. It is broad-band in nature and is distinct from the discrete tones observed during combustion instability. Instability occurs when feedback is established between unsteady combustion and pressure perturbations in a combustion chamber. The mechanism is that the unsteady combustion generates pressure waves, which reflect at the boundaries of the combustor and the velocity or equivalence perturbation associated with these waves causes more unsteady combustion. If the phase relationship is suitable [21,22], self-excited oscillations grow. This leads to discrete tones at resonant frequencies associated with the acoustic characteristics of the combustor and can be accompanied by high noise levels and severe pressure oscillations that can cause structural damage to engine components [5–7]. The vibrations induced by the oscillations can cause fatigue cracking of combustor liners and reduce the lifetime of a combustor by a factor

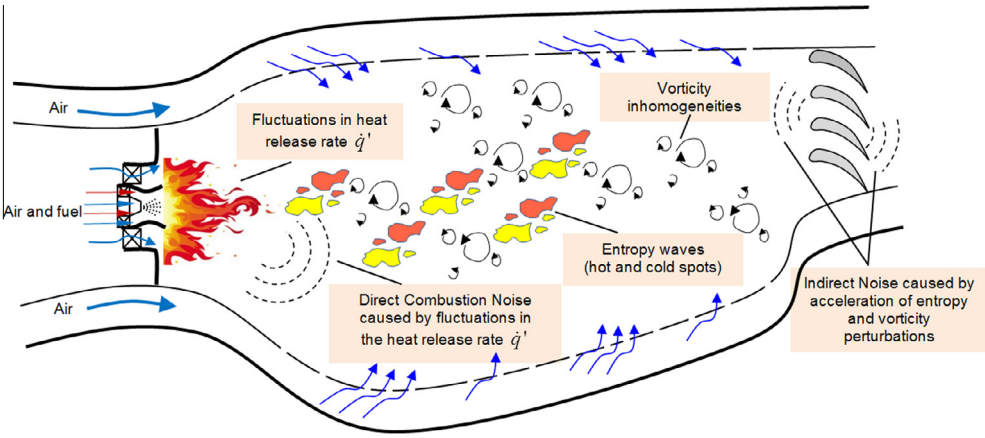

Fig. 3. Illustration of combustion noise sources in a gas turbine: generation of direct combustion noise and indirect combustion noise in aero-engines.

of two or more [6,23]. During an instability the heat release and the pressure perturbations throughout the combustor are at a fixed frequency and coherent.

In contrast, under normal stable operating conditions the combustion noise sources are incoherent throughout the combustor, and the combustion noise is a random output of turbulent combustion and radiates across a broadband of frequencies. However, some of the numerical and experimental techniques used to understand combustion instability are relevant to combustion noise, particularly the modelling of the linear waves (acoustic, entropic and vortical) generated by unsteady combustion within the complicated geometry of a gas turbine.

An additional link between broadband combustion noise and combustion instability is that the generation of pressure oscillations by entropy waves at the choked combustor, which is the main source of indirect combustion noise, has been studied extensively because it may play a role in the feedback mechanism for combustion instability [24–27]. Indeed pressure waves generated in this way are considered to be the key feedback-mechanism for a very low frequency combustion instability [24,26,28,29] called 'rumble'. Rumble usually only occurs at start-up of aero-engines at sub-idle and idle conditions, and exhibits such low frequencies (in the range of 50 Hz to 150 Hz) that it does not couple to the combustor acoustic resonances [28]. The feedback mechanism is thought to involve the entropy waves generated by the unsteady combustion convecting downstream to the combustor exit, where acceleration through the nozzle leads to an upstream propagating pressure wave which perturbs the combustion further. It is the long convection time from flame zone to combustor exit that leads to the low frequencies of self-excitation. The dissipation or dispersion of these entropy waves can stabilize or destabilize the modes of the system, depending on the configuration of the combustor and the form of the coupling [26,30].

In contrast to combustion instability, in broadband combustion noise the unsteadiness in the rate of combustion is mostly caused by the local turbulent flow and mixing, and is only very weakly influenced by reflected waves from the boundaries. Predicting the sources of both direct combustion noise and entropy noise requires an understanding of the characteristics of the underlying heat release fluctuations [10,31]. Thus, studies of combustion noise are inevitably linked to the understanding of combustion modes of flames. Previous investigations on combustion noise indicated that combustion noise is broadband having random phase and the peak intensity is typically in the low frequency range around 200–1000 [32–34].

This paper contains a review of progress in these various areas and a discussion of current challenges. It focuses on comparison between direct and indirect (entropy and vorticity) combustion noise. The classical theory of combustion noise of open flames is presented in Section 3. Section 4 presents the governing equation of combustion noise derived from the exact equations of conservation of mass, momentum and energy. It enables the different terms describing noise sources (direct combustion, accelerating entropy and vorticity) to be identified within a unified framework. Combustion noise of confined flames and comparison between direct and indirect (entropy and vorticity) is presented in Section 5. The challenges and unexplored issues in understanding the combustion noise are discussed in Section 6. To give more insight about the

generation mechanism of combustion noise, analytical solutions are presented in Section 7 for a model combustor based on a low Mach number approximation. The numerical procedure of linearized Euler equations based on the low-order thermo-acoustic network model (LOTAN) and the specific boundary conditions are briefly described in Section 8. Section 9 discusses the results obtained based on the analytical and numerical solutions. First the validity of the analytical solution, based on the low mean flow Mach number approximation, is tested against the numerical solution of the linearized Euler equations in a modal combustor. Then the effects of different parameters such as frequency, stagnation temperature ratio across the flame, and inlet Mach number on the magnitude of the acoustic, entropic and vortical waves are studied. Results for the choked outlet nozzle and the magnitude of indirect and direct noise generated are presented in Section 9.3 for a range of different frequencies, inlet Mach numbers and stagnation temperature ratios. Conclusions of the paper, open questions and possible areas for future research are presented in Section 10.

3. Classical theory of combustion noise

A classical experiment on noise emitted from combustion was conducted by Thomas and Williams [14] who filled a soap bubble with a homogeneous premixed fuel–air mixture and ignited it by a spark at the centre of bubble (see Fig. 4a). The constant pressure ignition produced a transient burning of mixture which resulted in a transient increase of the volume of bubble gases. As a consequence, a spherically symmetric pressure wave was emitted. Since the bubble size is small compared to the acoustic wavelength, this type of emission can be considered as a monopole point source of sound. The pressure in the sound wave emitted by the flame was recorded as a function of time, Fig. 4b, in which good quantitative agreement was obtained between the measured pressure field and that calculated by measuring and differentiating the bubble radius-time curves. They showed that the sound pressure depended linearly on flame radius and on the square of burning velocity. In this early study it was found that at a distance, r from the ignition position, the pressure fluctuation, $p'(r,t)$ was given by

$$p'(r,t) = \frac{\rho_0}{4\pi r}\ddot{V}(t - r/c_0), \tag{1}$$

where $V(t)$ is the volume of the bubble. ρ_0 and c_0 are the mean air density and speed of sound in far-field through which the sound is propagating. The prime denotes a perturbation from the mean and a dot a time derivative. Thus $\ddot{V}(t) = d^2V/dt^2$ is the second rate of change of the volume of the bubble. Equation (1) represents the fundamental principle of combustion noise: the sound is generated by unsteadiness in the rate of expansion by combustion of gas. In an open flame, it is the rate of change of the expansion rate that generates sound, $\ddot{V}(t)$. Steady combustion, leading to a constant rate of expansion, is silent. Although, in this simple experiment the flame was laminar, the results have been proven to be equally applicable to noise emission from open turbulent flames. In the phenomenological theory of Bragg [13] on direct combustion noise, it was assumed that the turbulent flame was a collection of eddies, which have their own heat release rate. Each eddy acts as a monopole source of sound which is statistically independent of the neighbouring eddies.

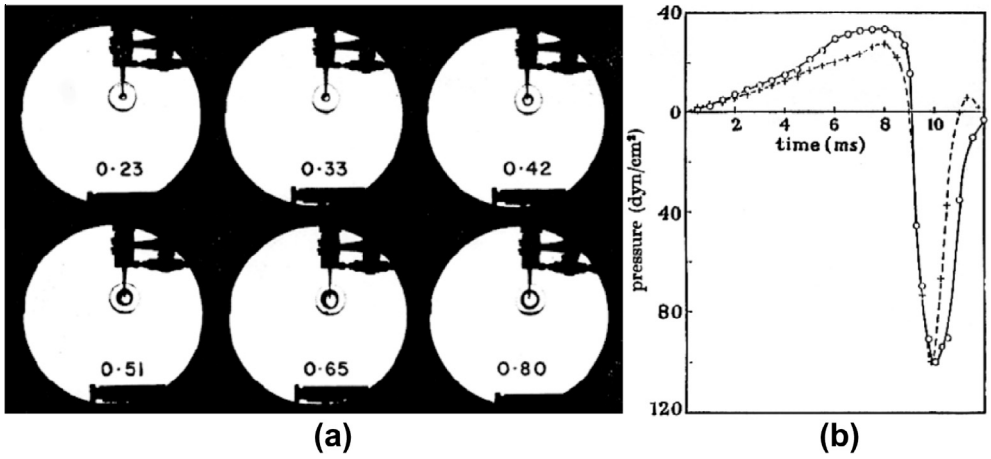

Fig. 4. (a) Instantaneous snapshots of an expanding spherical flame front after ignition in time and (b) acoustic pressure produced by expansion obtained for C_2H_4-O_2-N_2 mixture with burning velocity of 55 cm s^{-1}, + measured and o computed pressure (Thomas and Williams [14] by permission of the Royal Society).

Many studies (e.g. [11,35–37]) have tried to address the problem of combustion noise in turbulent flames and assumed that the turbulent flame can be regarded acoustically as an assembly of monopole sound sources with different strengths and phases that are distributed in the reaction zone of the flame. Price et al. [35] and Hurle et al. [36] found that the far-field sound pressure radiated by a turbulent premixed flame depends on the rate of volume increase of the fuel and oxidant in the combustion region, in which the rate of volume increase is proportional to the rate of consumption of the fuel and oxidant in the flame. Price et al. [35] also pointed out that the same result holds for turbulent diffusion flames, if it is assumed that the fuel and air burn in stoichiometric proportions. According to this model, it has been shown that the instantaneous sound pressure $p_i'(r,t)$ in the sound waves that emanate from the ith source element in the turbulent flame is given by

$$p_i'(r,t) = \frac{\rho_0}{4\pi r}(E-1)\ddot{v}_i(t-r/c_0), \tag{2}$$

where r is the distance of observer from the source, $\dot{v}_i$ is the volume rate of consumption of fuel and oxidant in the flame element and E is the volumetric expansion ratio of burned to unburned gases. For combustion at constant pressure E is equal to ρ_u/ρ_b where ρ_b and ρ_u are the mean density of the burnt and unburnt gases. They also commented that for a compact flame, the total sound pressure in the far field is given by the simple summation over all elements of the component pressures, $p_i'(r,t)$ in Eq. (2). Hurle et al. [36] confirmed this relationship experimentally by using the light emission from short-lived CH or C_2 free radicals to monitor the rate of combustion. Since their pioneering work, the relationship between acoustic pressure perturbation and rate of heat release in combustion has been verified using more advanced signal processing by Shivashankara et al. [38].

3.1. Far-field pressure distribution of an open turbulent flame

Consider an example of an open turbulent premixed flame shown in Fig. 5. Dowling and Ffowcs Williams [15] and Crighton et al. [39] showed that by using Lighthill's analogy [40] the far-field sound pressure fluctuation resulting from the direct noise is given by [15,39]

$$p'(\vec{x},t) = \frac{(\gamma-1)}{4\pi c_0^2|\vec{x}|}\int_v \ddot{q}(\vec{y},t-|\vec{x}|/c_0)d^3\vec{y}, \tag{3}$$

where v is the volume containing the combustion region or the flame brush. In the derivation of Eq. (3) $\vec{x}$ is considered to be in the far-field and the flame is compact. Then $r^{-1} = |\vec{x}-\vec{y}|^{-1}$ is approximately $|\vec{x}|^{-1}$ and the retarded time $t-|\vec{x}-\vec{y}|/c_0$ simplifies to $t-|\vec{x}|/c_0$ [39]. In this expression it has been assumed that γ the ratio of specific heats is independent of temperature and that the combustion takes place at ambient pressure, so that $\rho c^2 = \gamma p_0 = \rho_0 c_0^2$. Ambient conditions in the region surrounding the combustion region are denoted by the suffix 0 and $\dot{q}(\vec{y},t)$ is the instantaneous rate of heat release per unit volume in the combustion region. Equation (3) is valid in the far-field, i.e. for $|\vec{x}| >> |\vec{y}|$ and $|\vec{x}| >> c_0/\omega$, where ω is a typical radian frequency of the sound produced. The compact assumption requires that $|\vec{y}| << c_0/\omega$ for positions $\vec{y}$ within the combusting zone, i.e. the dimension of flame length is small compared with the acoustic wavelength/2π. The same expression as Eq. (3) for pressure perturbation has also been derived by Strahle [41] (Eq. (3) slightly differs from the original one derived by Strahle [41], who erroneously considered the monopole to be related to the rate of change of $\int_S \rho_b \vec{u}\bullet d\vec{S}$ rather $\rho_0\int_S \vec{u}\bullet d\vec{S}$, where S is any surface enclosing the combustion zone and $\vec{u}$ is the fluid velocity. Strahle's result should therefore be multiplied by the factor ρ_0/ρ_b).

Equation (3) clearly states that the rate of change in the total heat release rate generates pressure fluctuations. This expression applies to turbulent premixed, non-premixed and partially premixed flames as noted by Hurle et al. [36]. Although, the characteristics of heat release mechanisms and the physics underlying the combustion process in different modes affect the characteristics of pressure fluctuation, Eq. (3) clearly manifests that noise depends on the combustion mode through the temporal change of heat release rate in the combustion region [36,41].

For turbulent combustion, the acoustic pressure will be a stochastic variable and we are more interested in its statistical properties than any instantaneous value. The mean square pressure perturbation $\overline{p'^2(\vec{x})}$ can be obtained by squaring Eq. (3) and taking the time average. This leads to

$$\overline{p'^2(\vec{x})} = \left(\frac{\gamma-1}{4\pi c_0^2|\vec{x}|}\right)^2 \overline{\int \ddot{q}(\vec{y},t)d^3\vec{y} \times \int \ddot{q}(\vec{z},t)d^3\vec{z}},$$

where the overbar denotes a time mean. Substituting for $\vec{z} = \vec{y} + \vec{\Delta}$, where $\vec{\Delta}$ is the separation vector, results in

$$\overline{p'^2(\vec{x})} = \left(\frac{\gamma-1}{4\pi c_0^2|\vec{x}|}\right)^2 \int_v \int_{v_t} \overline{\ddot{q}(\vec{y},t)\ddot{q}(\vec{y}+\vec{\Delta},t)}d^3\vec{\Delta}d^3\vec{y}, \tag{4}$$

where v_t is the volume over which the integrand is non-zero. The ratio of the volume integral $\int \overline{\ddot{q}(\vec{y},t)\ddot{q}(\vec{y}+\vec{\Delta},t)}d^3\vec{\Delta}$ to the maximum value of its integrand $\overline{\ddot{q}^2(\vec{y},t)}$ is defined to be correlation volume, which we denote by $V_{cor}(\vec{y})$. It is the

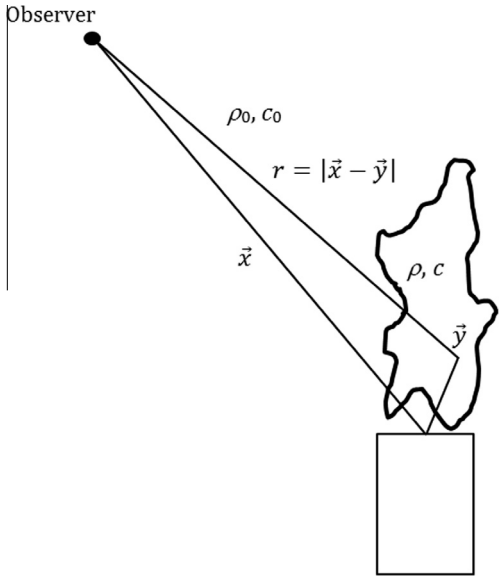

Fig. 5. Schematic of turbulent flame illustrating coordinates for the description of the acoustic field.

volume over which $\ddot{q}$ in the turbulent combustion is correlated. Writing

$$\int \overline{\ddot{q}(\vec{y},t)\ddot{q}(\vec{y}+\vec{\Delta},t)}d^3\vec{\Delta} = \overline{\ddot{q}^2(\vec{y},t)}V_{cor}(\vec{y}),$$

Equation (4) becomes

$$\overline{p'^2(\vec{x})} = \left(\frac{\gamma-1}{4\pi c_0^2|\vec{x}|}\right)^2 \int_v \overline{\ddot{q}^2(\vec{y},t)}V_{cor}(\vec{y})d^3\vec{y}. \qquad (5)$$

Equation (5) applies to any flame mode. It is clear that to predict the mean square far-field pressure perturbation we need to know $\overline{\ddot{q}^2(\vec{y},t)}$ and $V_{cor}(\vec{y})$. A flame is characterized by its mean rate of heat release $\bar{\dot{q}}(\vec{y})$ and there are well developed methods, computational and experimental, to determine this. From Eq. (5) we can decompose the requirements for modelling combustion noise of an open turbulent flame into the need to model the correlation volume $V_{cor}(\vec{y})$ and the way in which $\overline{\ddot{q}^2}(\vec{y})$ is related to $\bar{\dot{q}}(\vec{y})$. The ratio $\overline{\ddot{q}^2}(\vec{y})/\bar{\dot{q}}^2(\vec{y})$ can be rewritten as the product

$$\frac{\overline{\ddot{q}^2}(\vec{y})}{\overline{\dot{q}'^2}(\vec{y})} \times \frac{\overline{\dot{q}'^2}(\vec{y})}{\bar{\dot{q}}^2(\vec{y})}.$$

The first term is the ratio of the mean square value of the time derivative of $\dot{q}'(\vec{y},t)$ to the mean square value of $\dot{q}'(\vec{y},t)$ itself. Hence, it represents a frequency squared. The second term is the square of the rms value of $\dot{q}(\vec{y},t)$ to its mean, which is a non-dimensional measure of the amplitude of the perturbation.

Many scaling laws and empirical relations have been proposed to understand the physics of combustion noise. The acoustic pressure wave perturbation given by Eq. (5) can be applied to all modes of turbulent combustion, premixed [10,11,33,35,42–48], non-premixed [34,49–53] and partially premixed [54,55]. Candel et al. [10] give a review of empirical and computational modelling of the noise source for premixed flames. More recently for premixed flames Swaminathan et al. [31,56] and Liu et al. [57] have analysed Direct Numerical Solutions (DNS) and advanced laser diagnostics of premixed flames to obtain two-point spatial correlation of the rate of change of the fluctuating heat release rate. This approach leads to the development of a generic form for the cross-correlation. The results has then been applied to predict the far-field Sound Pressure Level (SPL) using Eq.(5) from open flames reported in [46].

The sound field from non-premixed and partially premixed flames is less well characterized than that radiated by premixed flames. This is due to the difficulty in modelling the rate of heat release and the complexity of measuring this quantity experimentally. Furthermore, in experiments the level of mixing of fuel and oxidizer would cause the generated sound to feature characteristics of premixed flame sound. Nonetheless, a number of investigations studied the combustion noise radiated by non-premixed [34,49–53] and partially premixed flames [54,55] to understand the region bridging these combustion modes. It was pointed out that higher levels of sound are generated by turbulent non-premixed flames than by premixed flames at a similar velocity [58]. For premixed flames, the region that the maximum acoustic output occurs are located close to the flame tip [37], while, for turbulent non-premixed flames predominant sound sources are distributed in the rear region of the reaction zone [35,58]. Further, using Mach number (M) scaling [54] it was demonstrated that the rms sound pressure generated by methane partially premixed flames scales with M^5 compared to M^3 for turbulent non-premixed methane flames.

4. General thermoacoustic sources and combustion noise

In Section 3 we picked out the dominant noise source when unsteady combustion occurs in an unbounded flow (Eq. (3)). But further insight can be obtained by working from the full equations of motion. In this way we are able to set combustion noise within a framework that extends to include jet noise and to identify entropy and vorticity as sources of sound. The starting point is Lighthill's equation [40,59]. Lighthill showed that the exact mass and momentum conservation equations can be written in the form [40,59]:

$$\frac{\partial^2\rho'}{\partial t^2}-c_0^2\frac{\partial^2\rho'}{\partial x_i\partial x_i}=\frac{\partial^2 T_{ij}}{\partial x_i\partial x_j} \tag{6}$$

where $\rho'=\rho-\rho_0$ and $T_{ij}=\rho u_i u_j+(p-p_0-c_0^2(\rho-\rho_0))\delta_{ij}-\tau_{ij}$ is the Lighthill stress tensor. The Kronecker delta is denoted by δ_{ij}. ρ is the density, p the pressure and $\vec{u}$ the particle velocity. ρ_0, p_0 and c_0 denote the mean density, pressure and speed of sound in the acoustic far-field. τ_{ij} is the viscous stress tensor. In a high Reynolds number isothermal flow T_{ij} reduces to $\rho u_i u_j$ showing that the unsteady Reynolds stresses generate sound in the same way as would a distribution of quadrupoles [39]. This is the basis of Lighthill's theory of jet noise. However, when there is combustion, there are significant regions of the flow where the density is significantly different from ambient and the term $c_0^2(\rho-\rho_0)\delta_{ij}$ within T_{ij} is important. Equation (6) can be rearranged to highlight this by arranging the wave operator to be on the pressure fluctuations and writing

$$\frac{1}{c_0^2}\frac{\partial^2 p'}{\partial t^2}-\frac{\partial^2 p'}{\partial x_i\partial x_i}=\frac{\partial^2}{\partial x_i\partial x_j}(\rho u_i u_j-\tau_{ij})-\frac{\partial^2\rho_e}{\partial t^2}, \tag{7}$$

where $\rho_e=\rho-\rho_0-(p-p_0)/c_0^2$ is the so-called 'excess density' [39]. This quantity vanishes in the far-field but is non-zero in regions where the entropy is significantly different from that in the surroundings. The thermoacoustic sound sources, $\partial^2\rho_e/\partial t^2$ and $\partial^2\tau_{ij}/\partial x_i\partial x_j$ are nonzero in the regions with irreversible processes. Viscosity is not a significant parameter in flow noise at least in regions away from the boundary layers, so that there is very little loss of generality in assuming flow motions to be inviscid. Thus, in Eq. (7) the viscous term $\partial^2\tau_{ij}/\partial x_i\partial x_j$ is small and can be ignored. Thermodynamic relationships can be used to determine the strength of the source $\partial^2\rho_e/\partial t^2$. The details are given by Dowling in Crighton et al. [39]. First, the partial time derivative is written in a form of material derivative as

$$\frac{\partial\rho_e}{\partial t}=\frac{D\rho_e}{Dt}-\frac{\rho_e}{\rho}\frac{D\rho}{Dt}-\frac{\partial(u_i\rho_e)}{\partial x_i}, \tag{8}$$

where the material derivative $D/Dt=\partial/\partial t+\vec{u}\bullet\nabla$ and the continuity equation has been used to replace $\partial u_i/\partial x_i$ with $-\rho^{-1}D\rho/Dt$. The energy equation for a gas made up of N chemically reacting species results in [31,39]

$$\frac{D\rho}{Dt}=\frac{1}{c_0^2}\frac{Dp}{Dt}+\frac{\alpha}{c_p}\left(\frac{\partial q_i}{\partial x_i}-\tau_{ij}\frac{\partial u_i}{\partial x_j}+\sum_{n=1}^{N}\left.\frac{\partial h}{\partial Y_n}\right|_{\rho,p,Y_m}\rho\frac{DY_n}{Dt}\right), \tag{9}$$

where Y_n is the mass fraction of the nth species, h the enthalpy and q_i is the heat flux vector given by $q_i=-k\partial T/\partial x_i+\rho\sum_{n=1}^{N}Y_n h_n V_{n,i}$ with k the thermal conductivity of the mixture and $V_{n,i}$ the diffusion velocity of the nth species in direction i. The specific heat at constant pressure is c_p, the volumetric expansion coefficient is α and for an ideal gas is equal to $1/T$, and $\alpha/c_p=(\gamma-1)/c_0^2$. Equation (9) demonstrates that the density of a material particle changes because of the pressure variations in a compressible fluid and also because of the expansion caused by heating. If ρ_e in Eq. (8) is written explicitly as $\rho-\rho_0-(p-p_0)/c_0^2$, Eq. (9) can be used to replace $D\rho/Dt$ this leads to

$$\frac{\partial\rho_e}{\partial t}=\frac{\alpha\rho_0}{c_p\rho}\left(\frac{\partial q_i}{\partial x_i}-\tau_{ij}\frac{\partial u_i}{\partial x_j}+\sum_{n=1}^{N}\left.\frac{\partial h}{\partial Y_n}\right|_{\rho,p,Y_m}\rho\frac{DY_n}{Dt}\right)-\frac{\partial(u_i\rho_e)}{\partial x_i}-\frac{1}{c_0^2}\left[\left(1-\frac{\rho_0 c_0^2}{\rho c^2}\right)\frac{Dp}{Dt}-\frac{(p-p_0)}{\rho}\frac{D\rho}{Dt}\right].$$

Substituting into Eq. (7) results in

$$\begin{aligned}\frac{1}{c_0^2}\frac{\partial^2 p'}{\partial t^2}-\frac{\partial^2 p'}{\partial x_i\partial x_i}&=-\frac{\partial}{\partial t}\left[\frac{\alpha\rho_0}{c_p\rho}\left(\sum_{n=1}^{N}\left.\frac{\partial h}{\partial Y_n}\right|_{\rho,p,Y_m}\rho\frac{DY_n}{Dt}+\frac{\partial q_i}{\partial x_i}-\tau_{ij}\frac{\partial u_i}{\partial x_j}\right)\right]\\&\quad+\frac{\partial^2}{\partial x_i\partial x_j}(\rho u_i u_j-\tau_{ij})+\frac{1}{c_0^2}\frac{\partial}{\partial t}\left[\left(1-\frac{\rho_0 c_0^2}{\rho c^2}\right)\frac{Dp}{Dt}-\frac{(p-p_0)}{\rho}\frac{D\rho}{Dt}\right]+\frac{\partial^2}{\partial x_i\partial t}(u_i\rho_e).\end{aligned} \tag{10}$$

Using the chain rule of differentiation

$$\begin{aligned}\sum_{n=1}^{N}\left.\frac{\partial h}{\partial Y_n}\right|_{\rho,p,Y_m}\rho\frac{DY_n}{Dt}&=\sum_{n=1}^{N}\left.\frac{\partial h}{\partial Y_n}\right|_{T,p,Y_m}\omega_n-\left.\frac{\partial h}{\partial\rho}\right|_{p,Y_n}\left(\sum_{n=1}^{N}\left.\frac{\partial\rho}{\partial Y_n}\right|_{T,p,Y_m}\omega_n\right)\\&\quad-\sum_{n=1}^{N}\left.\frac{\partial h}{\partial Y_n}\right|_{\rho,p,Y_m}\nabla J_n,\end{aligned} \tag{11}$$

where ω_n is the production rate per unit volume of species n by reaction, and $J_{n,i}=\rho V_{n,i}Y_n$ is the flux of species n by diffusion in the direction i. The first term on the right hand side of Eq. (11) represents the heat release rate per unit volume and the second term describes the volumetric expansion due to non-isomolar combustion. The third term is determined by the effects due to species diffusion.

Truffaut et al. [60] examined the additional source of noise associated with non-isomolar combustion described by the second term on the right-hand side of Eq. (11). When fuels are burnt in air, the reactive species are strongly diluted in inert nitrogen and the contribution of molar expansion is small compared to the direct heat release term (the first term of the right-hand side of Eq. (11)). Thus, for air-breathing combustion systems the molar production term can be neglected [61]. However in some industrial applications, such as welding torches, fuels are burnt in pure oxygen and then the change in the number of moles is no longer negligible, partly because the chemical species are no longer diluted in nitrogen

but also because the high combustion temperature (>3000 K) leads to strongly dissociated combustion products [60].

Substituting Eq. (11) into Eq. (10) leads to an inhomogeneous wave equation which can be written as

$$\frac{1}{c_0^2}\frac{\partial^2 p'}{\partial t^2}-\frac{\partial^2 p'}{\partial x_i \partial x_i}=\dot{W}_1+W_2+\dot{W}_3+\dot{W}_4, \tag{12a}$$

where

$$W_1=-\frac{\alpha\rho_0}{c_p\rho}\left(\sum_{n=1}^{N}\left.\frac{\partial h}{\partial Y_n}\right|_{T,p,Y_m}\omega_n-\left.\frac{\partial h}{\partial \rho}\right|_{p,Y_n}\times\left(\sum_{n=1}^{N}\left.\frac{\partial \rho}{\partial Y_n}\right|_{T,p,Y_m}\omega_n\right)-\sum_{n=1}^{N}\left.\frac{\partial h}{\partial Y_n}\right|_{\rho,p,Y_m}\nabla.J_n+\frac{\partial q_i}{\partial x_i}-\tau_{ij}\frac{\partial u_i}{\partial x_j}\right), \tag{12b}$$

$$W_2=\frac{\partial^2}{\partial x_i \partial x_j}(\rho u_i u_j-\tau_{ij}), \tag{12c}$$

$$W_3=\frac{1}{c_0^2}\left(\left(1-\frac{\rho_0 c_0^2}{\rho c^2}\right)\frac{Dp}{Dt}-\frac{(p-p_0)}{\rho}\frac{D\rho}{Dt}\right), \tag{12d}$$

$$W_4=\frac{\partial}{\partial x_i}(u_i\rho_e) \tag{12e}$$

The details of the derivation of this equation are given explicitly by Dowling in Crighton et al. [39]. Bailly et al. [62] obtained a similar equation based on an extension of Lilley's equation [63] to reactive flows. Lilley's equation includes some mean flow propagation effects with propagation through a parallel mean shear flow being included in the operator on the left-hand side of the equation.

Assuming that the terms on the right hand side of Eq. (12a) are known, the problem is equivalent to an inhomogeneous wave equation. These terms represent the various sources of sound generation. The first term W_1 is of monopole type and describes the sound generated by irreversible flow processes from the unsteady heat release rate and those of non-isomolar combustion, species diffusion, heat diffusion and viscous dissipation [64,65]. When exothermic reactions take place, the first term in Eq. (12b) due to the rate of heat release is the most significant. The term $\nabla\bullet\vec{q}$ in Eq. (12b) is the heat-conduction noise source, discussed by Sinai [66]. The second term W_2 is the familiar quadrupole source of Lighthill's jet-noise theory associated with the velocity fluctuations. It is well known that it leads to an acoustic intensity that scales with Mach number to the eight power, M^8 [39]. As noted by Powell [67], in a low Mach number isothermal flow W_2 is approximately equal to $\nabla\bullet(\rho\vec{\omega}\times\vec{u})+\nabla^2\left(\frac{1}{2}\rho|\vec{u}|^2\right)$. It is this source that generates sound when vorticity is accelerated and, when combustion occurs in a confined geometry with a downstream constriction, leads to the indirect combustion noise source we introduced in Section 2. We will discuss this further in Section 5. The third term W_3 also leads to an M^8 scaling [39] but with a different coefficient from the classical Lighthill's term. It is only appreciable if ρc^2 in the combustion region is not equal to $\rho_0 c_0^2$, the value in the far-field. Since $\rho c^2=\gamma p$ and pressure is nearly constant throughout a low Mach number flow, this noise source should be very small [10]. As pointed out by Sinai this term is only effectively nonzero in a fluid with variations in its specific heats and even then he found that this mechanism of noise generation to be insignificant [66]. The last term W_4 is dipole in nature and describes the effect of momentum changes on density inhomogeneities; it is the entropy noise source discussed in Section 2.

In the combustion region ω_n the rate of production species n is nonzero and the first term on the right hand side of Eq. (12a) describes the strong monopole sound source of combustion [39]. It has been shown by Flemming et al. [52] and Ihme et al. [53] that when unsteady combustion occurs in a low Mach number flow, this term is about two orders of magnitude larger than the other sources demonstrated in Eq. (12a). If the average molecular weight is constant, the second term in the first part of Eq. (12a) is neglected. When the diffusion of species in neglected then for the combustion of hydrocarbons in air

$$-\sum_{n=1}^{N}\left.\frac{\partial h}{\partial Y_n}\right|_{\rho,p,Y_m}\omega_n=\dot{q}, \tag{13}$$

where $\dot{q}$ is the heat release rate per unit volume. For an ideal gas $\alpha/c_p=(\gamma-1)/c^2$. If γ is assumed to be independent of temperature and the combustion takes place at ambient pressure, as is the case for example in an open turbulent flame then we have $\rho c^2=\gamma p_0=\rho_0 c_0^2$. Then applying Eq. (13) into Eq. (12a) results in an equation for combustion noise as

$$\frac{1}{c_0^2}\frac{\partial^2 p'}{\partial t^2}-\frac{\partial^2 p'}{\partial x_i^2}=\frac{(\gamma-1)}{c_0^2}\ddot{q}(\vec{y},t). \tag{14}$$

Using the free-space Green function [39] gives the far-field pressure perturbation due to an open flame as

$$4\pi c_0^2|\vec{x}|p'(\vec{x},t)=(\gamma-1)\int_v \ddot{q}(\vec{y},t-|\vec{x}|/c_0)d^3\vec{y}, \tag{15}$$

recovering the result of the simplified analysis in Eq. (3). Equation (15) predicts that in the far-field for a compact flame, i.e. when the wavelength of the emitted sound is large compared to the flame length, the acoustic pressure perturbation is proportional to the time derivative of the total heat release evaluated at a retarded time. The variations of γ arising due to temperature inhomogeneities

can generate monopole sound when it is subjected to pressure fluctuations, as noted by Dowling [68], Strahle [69] and Sinai [66], but this effect is negligible compared to the strong combustion source in Eq. (15). In free space, the contributions from the entropy and vorticity terms (in Eqs. (12e) and (12c)) are also smaller than the term retained in Eq. (15) but they can have significant effects when there are strong variations in the mean flow. Additional combustion noise is generated when these entropy perturbations are accelerated by the flow through constrictions in an engine [11,18]. The relative contribution to the overall radiated noise from indirect and direct combustion noise components is an ongoing issue [9,10] that we examine further in the following sections.

5. Combustion noise of confined flames

In practical applications it is more common for combustion to be confined than to occur in unbounded space. We introduce the noise of confined flames by investigating the first the small amplitude flow perturbations that can occur in the flow through a duct/pipe of constant cross-sectional area with uniform mean flow properties. Dowling and Stow [5] showed that by rewriting the flow properties as a sum of time-averaged (denoted by an overbar) and fluctuating (denoted by a prime) components, the linearized conservation equations maybe rearranged to describe the development of acoustic, entropy and vorticity fluctuations. It was shown that with no heat source, any linear perturbation can be thought of as the sum of three types of disturbances [5], (i) an acoustic disturbance that is isentropic and irrotational; (ii) an entropic disturbance that is incompressible and irrotational; and (iii) a vortical disturbance that is incompressible and isentropic. These three types of disturbances are independent and when linear can be considered separately and superimposed [5]. Acoustic disturbances involve velocity, pressure, density, and temperature fluctuations. For the acoustic disturbance the entropic and vortical fluctuations are zero, i.e. $S' = 0$ and $\vec{\xi}' = 0$, hence

$$\left(\frac{1}{c_0^2}\frac{D_1^2}{Dt^2} - \nabla^2\right)p' = 0, \tag{16}$$

where D_1/Dt is the convected derivative $\partial/\partial t + \vec{\bar{u}} \bullet \nabla$ and $\vec{\bar{u}}$ is the mean fluid velocity assumed to be uniform. Disturbances of this type are acoustic waves and, relative to the fluid, they propagate at the speed of sound.

The entropic disturbances do not involve fluid motion or pressure disturbances. They consist of temperature and density fluctuations. Incompressible and irrotational entropy fluctuations, i.e. $p' = 0$ and $\vec{u}' = 0$, are expressed as

$$\frac{D_1 S'}{Dt} = 0. \tag{17}$$

This disturbance is stationary relative to the fluid, that is, it is convected with the mean flow. This disturbance can be thought of as an entropy wave, and is sometimes referred to as a 'convected hot spot'.

Vortical waves consist purely of vortical fluid motion without pressure, density, and temperature perturbations. For the vortical disturbance, $p' = \rho' = 0$ and hence the development of these incompressible and isentropic vorticity fluctuations are described by

$$\frac{D_1 \vec{\xi}'}{Dt} = 0. \tag{18}$$

The vorticity wave also convects with the mean flow.

The linearized governing equations for these three types of perturbations indicate that they are uncoupled in an uniform mean flow, and that the acoustic waves propagate with the speed of sound relative to the mean flow, whilst entropy and vorticity fluctuations are advected with the mean flow. If the mean flow is zero, the entropic and vortical waves do not convect and only the acoustic waves propagate. Using the full nonlinear Navier–Stokes equations, Chu and Kovásznay [19] analyzed the interaction of these three waves. They found that in a quiescent medium the interaction would be a second-order effect [19]. The entropy mode, which is silent in a uniform mean flow, may transfer energy to acoustic and vorticity modes and vice versa by a nonlinear interaction. When spatial gradients in steady flow properties exist, such as a combustion zone or the acceleration of the mean flow through a nozzle, all three types of linear waves can become coupled [70]. Palies et al. [70] investigated a vorticity wave generated by such an acoustic wave incident on an aerofoil cascade. The interaction of perturbations with blade rows has been extensively investigated in the field of turbomachinery, see for example the classical textbook of Horlock [71] and references ([72–74]). Acoustic waves can also be generated as entropy waves are convected by the mean flow through a nozzle [18,75]. Conversion of entropy fluctuations by a cascade has been worked out analytically by Cumpsty and Marble [76] and Cumpsty [77]. It is shown in these references that the interaction gives rise to acoustic pressure waves.

Many real combustion chambers feature choked exit nozzles. Numerous studies in the past have studied reflection and generation of sound by the passage of acoustic and entropic perturbations through a nozzle in the linear (e.g. [12,18,26,78–80]) and nonlinear regime [81,82] and for a broad range of frequencies. At mid to high frequencies, the wavelength of the entropy perturbations, i.e.

$2\pi|\overline{u}|/\omega$, is small compared with the turbulent length scale. Thus, these perturbations diffuse due to high turbulent mixing in the burned gases before the nozzle guide vanes and hence have negligible amplitude by the time they reach the nozzle [83,84]. Whilst, for low frequencies below a few hundred Hz, entropy perturbations have long wavelengths compared with the turbulent length scale. Hence, although these perturbations are also subjected to intense turbulent mixing, there is no significant diffusion nor dissipation of such entropy perturbations as they convect between the flame region to turbine inlet [82]. Further, recent studies have shown both numerically and experimentally the significance of entropy noise as a feedback for combustion instabilities and thermo-acoustic oscillations [26,85–87]. Thus, we know that at these lower frequencies entropy perturbations persist to the nozzle guide vanes with significant amplitudes.

In the linear regime, the response of the combustor exit to incoming perturbations has been studied theoretically by Marble and Candel [12]. They considered the choked nozzle to be one-dimensional and compact, an approximation that works well when all wavelengths are much longer than the nozzle. They derived analytical expressions for the relationship between the amplitude of the acoustic waves generated and the temperature fluctuations of the incident entropy waves. The generation of acoustic waves is determined by the condition that the non-dimensional mass flow rate be constant at the choked end. The indirect combustion noise is therefore related to the unsteady mass flux that must occur when temperature inhomogeneities enter the outlet throat. The compact nozzle theory of Marble and Candel [12] was extended by Cumpsty and Marble [76,88] and Cumpsty [77] to study entropy noise produced in a gas turbine at the combustor outlet and turbine blade stages. A significant increase of entropy noise generation was found with the increase of pressure drop over a turbine stage. Stow et al. [79] studied both analytically and numerically the reflection and transmission of downstream propagating acoustic, entropy and vorticity waves incident on a choked exit nozzle. They reported that for a compact choked nozzle the boundary condition of Marble and Candel [12] is applicable even for circumferential waves.

Bohn [80] investigated the one-dimensional response of a subsonic nozzle flow to pressure and entropy disturbances and pointed out the importance of nozzle shape on the noise generated at higher frequencies when the nozzle is no longer compact [80]. Stow et al. [79] and in a separate study Goh and Morgans [30] extended the compact solution of Marble and Candel [12] from low to mid frequencies through an asymptotic expansion of the linearized Euler equations for non-compact nozzles. They showed that the reflection and transmission across a nozzle can be extended to non-zero frequencies using an effective nozzle length that depends on the mean flow through the nozzle and hence on the nozzle shape. Moase et al. [89], for choked nozzle and supersonic diffusers, and Giauque et al. [90], for subcritical nozzles, extended the approach of Marble and Candel [12] to non-compact nozzles by solving the linearized Euler equations. They computed the linear transfer functions for the upstream and downstream acoustic waves generated by an incident entropy disturbance. Duran and Moreau [91] studied analytically the acoustic and entropy transfer functions of quasi-one-dimensional nozzles for both subsonic and choked flows with and without shock waves. Their study extended both the compact nozzle solution obtained by Marble and Candel [12] and the effective nozzle length proposed by Stow et al. [79] and by Goh & Morgans [30] to arbitrary frequencies through an asymptotic expansion of the linearized Euler equations. Their study can be applied to any nozzle geometry and different flow conditions. They found that for both choked and subsonic flows, the modulus and the phase of the transfer functions of linear waves across the nozzle have a strong dependence on the frequency.

Bloy [81] investigated the non-linear regime using the method of characteristics in one-dimensional flow and calculated the pressure fluctuations generated by the convection of a temperature disturbance (entropy wave) with low frequency and large amplitude passing through a subsonic nozzle. Huet and Giauque [82] also extended the compact nozzle model of Marble and Candel [12] to the nonlinear domain in order to study the generation of sound by the passage of acoustic or entropy perturbations through a nozzle in the low frequency limit. The accuracy of their proposed second order model for large amplitude entropy perturbations was evaluated by varying the inlet and outlet Mach numbers of the nozzle. They found that it is accurate for a supercritical nozzle for both types of waves considered.

Leyko et al. [78] used a simple quasi-1-D combustor model for an aero-engine terminated by a choked nozzle with the assumption of isentropic mean flow and quantified both direct and indirect noise. The analysis performed was in a cold flame, a simplification in which a flame is considered to generate only fluctuations in heat release, with no mean rate of heat release. With this simplification, the mean flow conditions upstream and downstream of the flame were assumed to be the same. They showed that the linearized acoustic theory of Marble and Candel [12] agrees well at low frequencies with the numerical results obtained by solving the Euler equations of motion. Further, they [78] showed that the ratio of indirect-to-direct noise depends on the Mach

number in the flame zone and the Mach number at the nozzle outlet (see Fig. 6). This ratio is small for laboratory experiments but large in most real aeroengines, indicating that indirect noise is then the dominant source and can exceed the direct noise by one order of magnitude but is negligible in most laboratory experiments [78].

In an extension to the work done by Leyko et al. [78], Duran and Moreau [91] studied the ratio of indirect to direct noise in a cold flame for different frequencies and Mach numbers. They produced a generalization of the indirect to direct noise ratio for different frequencies and concluded that for high frequencies, the indirect to direct noise ratio decreases as frequency increases, which means indirect noise is only significant at low frequencies and could be neglected at high frequencies. Using coherence analysis, Muthukrishnan et al. [92] deduced from experiments on a test rig for an aero-engine combustor that broadband indirect entropy noise is the principal source of the engine core noise if the combustor is choked at the exit. But up until now, there has been little systematic direct experimental proof of the importance of entropy noise in the ambient noise radiated from a complete aeroengine. This is presumably because of the difficulty of separating the different noise generating processes leading to direct and indirect combustion noise. To do this, an experiment, generating entropy waves by electrical heaters was performed by Bohn [80] and Zukoski and Auerbach [93] in seventies. In these experiments, however, the amplitude of the induced temperature fluctuation generated was too low (only about 1 K), there was little scope for parametric variations, and the data acquisition and processing system did not have a sufficiently high-resolution to separate out the direct and indirect noise components. The problem was studied again recently when Deutsches Zentrum für Luft- und Raumfahrt (DLR) built a small-scale generic test rig Entropy Wave Generator (EWG) [94–96] and Vorticity Wave Generator (VWG) [97] to study the indirect combustion noise. They showed that small non-uniformities of temperature can indeed generate significant noise when accelerated within a nozzle.

Figure 7a shows the experimental measurements of Bake et al. [95] for the amplitude of the generated sound pressure versus the amplitude of the temperature fluctuation for two nozzle Mach numbers. This figure confirms the linearized approach of Marble and Candel [12] in which the amplitude of the generated entropy noise is assumed to increase linearly with the amplitude of the temperature pulse. They also investigated the variation of the amplitude of the generated pressure wave for fixed inlet temperature variation as the mean inlet nozzle Mach number increased. The results are shown in Fig. 7b and demonstrate that the pressure amplitude increased nonlinearly with an increase of nozzle Mach number up to a certain amount (Fig. 7b). Further increase in Mach number resulted in decrease of the pressure wave amplitude [95].

The DLR experiment generated interest in the community and initiated multiple theoretical and numerical methods to explain the experimental results [78,98–101]. Leyko et al. [99] studied numerically and analytically the DLR experiments in an axisymmetric and a fully three-dimensional configuration. They reported that the linear acoustic and the low frequency compact nozzle hypothesis of Marble and Candel [12] is applicable for the experimental results of EWG of DLR [95]. They also demonstrated that the pressure signals measured in the DLR experiment result from the conversion of entropy perturbations into acoustic waves due the strong mean velocity gradient in the nozzle, as well as from the acoustic wave reflection with exhaust system downstream of the nozzle at the outlet [99]. The EWG has also been studied numerically using three-dimensional compressible URANS by Mühlbauer et al. [100]. The pressure fluctuations and spectra they calculated agreed well with the experiments in the EWG. They pointed out that the minor discrepancies between their simulation and the experiments could be removed by using a time-domain application of the measured impedance boundary condition describing acoustics of the exhaust as a function of the frequency. In contrast to the supersonic nozzles and subsonic convergent nozzles studied in [78], a subsonic configuration has been studied by Giauque et al. [90] and Duràn et al. [102]. The analytical results of Duràn et al. [102] based on a compact nozzle hypothesis for unchoked subsonic nozzle (with throat Mach number of 0.7) showed that the strength of indirect noise is two orders of magnitude smaller than the direct noise suggesting that the measured pressure waves at the outlet of EWG were not caused by entropy waves but rather by the acoustic waves generated by the heating device. Their numerical results for an unchoked subsonic nozzle based on non-compact nozzle theory illustrated that the strength of indirect noise increases with frequency and the compact nozzle solution is only correct for very small Helmholtz number, $f\ell/\bar{c}$ (zero frequencies) where ℓ is the nozzle length [102]. However, Leyko et al. [78] showed that the compact hypothesis is valid for dimensionless frequencies up to $f\ell/\bar{c} = 0.2$ for supersonic and subsonic convergent nozzles.

With the aim of calculating the combustion-generated noise at the outlet of the aero-engine, Leyko et al. [103] and Duràn et al. [104] combined LES with analytical models of Cumpsty and Marble [88] and applied them to an isolated blade row to differentiate the contribution of direct and indirect noise sources. Mishra and Bodony [105]

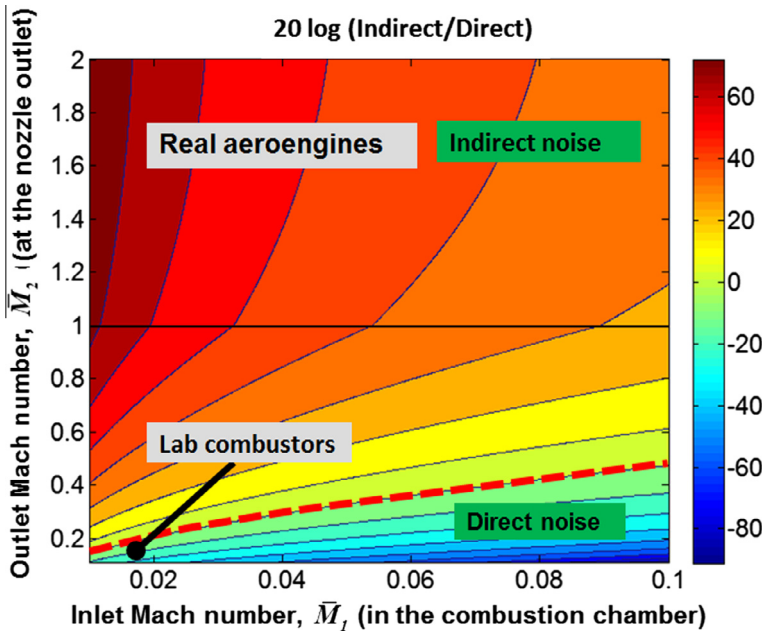

Fig. 6. Evaluation of the ratio of indirect to direct noise generated by a model combustor with a compact isentropic downstream nozzle. The noise is calculated in the downstream duct (based on Eqs. (34) and (35) in Leyko et al. [78]).

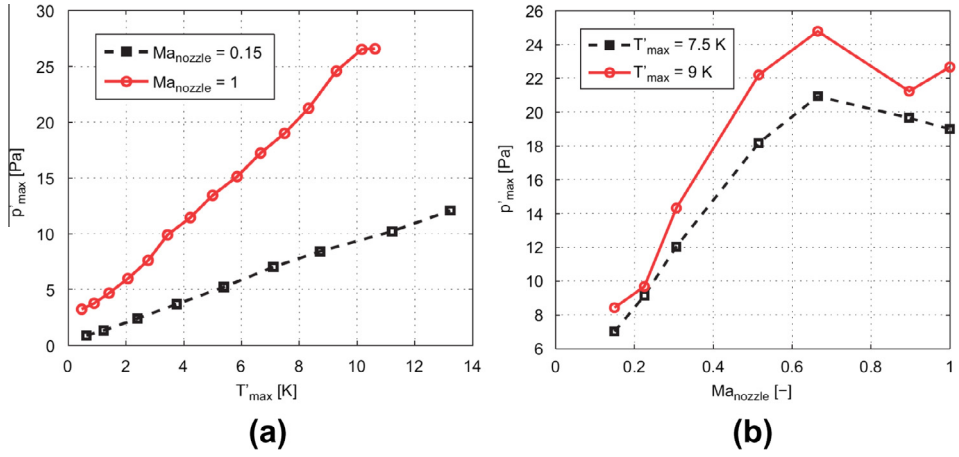

Fig. 7. (a) Acoustic pressure amplitude of generated entropy noise as a function of temperature perturbation for two different nozzle Mach numbers M = 0.15 and 1; (b) acoustic pressure wave versus nozzle Mach number for two different amplitudes of temperature perturbation [95].

also studied application of actuator disk theory numerically by comparison of two-dimensional simulations with the analytical model of Cumpsty and Marble [88] in the presence of small amplitude entropy perturbations. They [103–105] determined the limits of the compact nozzle model for a wide range of frequencies and evaluated the indirect combustion noise as entropy waves convect through stator and rotor blade rows.

6. Current challenges

It is noted that currently there is, in general, little agreement on the importance of indirect noise to the problem of combustion noise. This perhaps stems from a number of issues on understanding and modelling of entropic and vortical waves in combusting flows. For instance, hitherto, the output of the combustion chamber in terms of

acoustic (direct combustion noise), entropic (convecting hot and cold spots) and vortical perturbations (convecting vortex structures) has not been well characterized. The relative magnitudes of the waves generated by unsteady combustion certainly depend on the frequency and mean flow conditions. Furthermore, the decay of entropy and vorticity perturbations in a combustion chamber is not clear. In addition, the general problem of indirect noise requires that the impedance condition and transmission property at the combustor choked outlet be known. Incident entropy and vorticity waves cause both reflection and transmission of acoustic waves. But the reflected waves come back into the combustor where they reflect from both the flame zone and the combustor inlet. On occasion, they can even perturb the rate of combustion, which can contribute to a thermoacoustic instability. Hence, the transmission and reflection of indirect noise needs to be evaluated. The difficulties in solving these issues may be broadly summarized specifically as follows:

- Limitations in the modelling of the exit nozzle dynamics as the convertor of entropic and vortical disturbances into acoustic waves;
- Little quantitative information on the dissipation of entropy and vortical waves;
- Lack of a comprehensive understanding of the generation of linear waves in reactive flows.

6.1. Exit nozzle dynamics

The analytical derivations of Marble and Candel [12] and the extensions described in Section 5 have been the main tools to model the response of choked exits. These models assume a mean flow uniform over the cross-sectional area and only axial and circumferential perturbations. Although Leyko et al. [78] have shown that they work well on the one-dimensional mean flow of the experiment of Bake et al. [95] their experimental validation on geometries representative of aeroengine combustors is currently very limited.

Hield and Brear [106] extended the two microphone method of Seybert and Ross [107] by adding a thermocouple to the measurement system to quantify the incident entropy wave and so be able to investigate of the nozzle response to an entropic disturbance. They [106] applied this new method to both an open and a choked exit of a premixed combustor with a bluff-body flame stabiliser undergoing thermo-acoustic limit cycles. For the open exit, the acoustic reflection showed good agreement with the classical theory. However, in the case of the choked exit neither the reflected pressure or entropy response agreed with Marble and Candel's [12] linear boundary condition. It was argued that this may be expected, given the large amplitude of the forcing and the possible nonlinearity of the choked exit due to periodic nozzle unchoking, as suggested by Moase et al. [89].

The Marble and Candel [12] theory neglects any radial variation in the mean and unsteady flow field. While three-dimensional disturbances were investigated by Crocco and Sirignano [108] further work would be needed if incident three-dimensional disturbances are important in aeroengine combustors. There is an urgent need for experiments on aeroengine combustors, where the mean flow will vary around the annulus and across the radius, to enable the boundary conditions to be validated.

6.2. Dispersion of entropy waves

Between the flame, where the entropy waves are generated, and a choked combustor exit, these waves are convected by a flow that is non-uniform over the combustor cross-section and has intense turbulent fluctuations. As stated by Sattelmayer [84], the non-uniformity in the mean-flow profile leads to residence times that vary across the cross-section. Thus, entropy disturbances generated at different radial positions arrive at the nozzle with different time delays and hence phases. This will tend to reduce their cumulative effect and hence reduce the reflected acoustic wave, an effect that is more important at high frequencies. Sattelmayer's study [84] considers some essential physics of the dispersion problem. Partial diffusion of these waves changes their relative phase and influences the sound generation generated by their interaction with the nozzle, which can modify the resultant entropy noise [84]. The turbulence in the flow can also diffuse the entropy disturbances and therefore reduce their potential for sound generation. The importance of the dispersion of entropy waves has been noted by a number of authors [5,84,106,109]. However, these effects have not been considered in simplified analytical and numerical models of entropy noise (e.g. [12,30,78,89,91]). Thus, attempts to analyse this effect are quite rare.

Very recently Morgans et al. [109] studied entropy wave advection within a turbulent channel-flow. The study was based on Direct Numerical Simulation of entropy wave convection within a simplified fully-developed turbulent flow between two parallel plates. The effect of heat addition due to combustion was neglected, the coefficient of transport phenomena was considered to be constant, and the flow assumed to be incompressible. Thus, the acoustic fluctuations were assumed to be negligible and the temperature and entropy fluctuations scale with one another. They introduced a Gaussian perturbation in the temperature field at the inlet of the channel and studied the transport of the entropy fluctuations [109]. They found the entropy wave dissipation to be

negligible between the flame position and the end of the combustor. They pointed out that loss in entropy wave strength during differential convection by a mean flow which varies across a combustor cross-section will in practice be more important in a real aeroengine combustor [109]. Nevertheless, because of the general complexity of transport and diffusion in turbulent exhaust flows some important aspects of the problem are still unexplored and most of the current understanding of the dispersion process is rather intuitive.

6.3. Dynamics of linear wave generation

Survival of entropy waves throughout the combustor is influenced by both dispersion and by the initial strength of the disturbance. Those disturbances with larger initial amplitude have naturally a better chance of reaching the exit nozzle. The relative strengths of the pressure and entropic waves generated by unsteady combustion depend on the frequency and on the mean flow. A flame generates stronger entropy disturbances at low frequencies [110]. The current modelling of entropy generation invariably assumes that the disturbances are one-dimensional [5]. Thus the dynamics of entropy generation become a function of the global heat release. The spatial variation of entropy generation within the flame region is ignored. While this might be a reasonable approximation for laboratory experiments which have combustion within cylindrical tubes, aeroengine combustors are usually annular and combustion noise is important at frequencies where the first circumferential acoustic mode around the annular propagates. The unsteady combustion can therefore excite disturbances which vary with azimuthal angle around the circumference. In the next following sections we will investigate linear wave generation and reflection in annular combustors.

7. Analytical study of combustion noise

In this section we will discuss the general solution for linear unsteady flow in a cylindrical or annular duct of uniform cross-sectional area. It can be thought of as a sum of acoustic, entropic and vortical waves. We then determine the generation of these waves by unsteady heat input and compare their relative magnitudes.

7.1. Linear waves in an annular duct

We consider the form of perturbations that occur in the gap between two concentric cylinders. The straight duct is assumed to have cross-sectional area a, and the mean flow is axial and independent of circumferential or radial position. The flow is assumed to be inviscid, with pressure p, density ρ and velocity $\vec{u}$. We will assume a perfect gas, $p = R_{gas}\rho T$, and so, T may be written in terms of p and ρ. A linear disturbance in a straight duct can be thought of a sum of acoustic, entropy and vorticity waves, with acoustic waves propagating both upstream and downstream, while entropy and vorticity disturbances convect with the mean flow. Using cylindrical polar coordinates, x,r,θ, the velocity field is denoted by $\vec{u} = (u, v, w)$ and the duct has inner and outer mean radii r_i and r_o, respectively. In annular gas turbines, the radial gap $r_o - r_i$ of the combustor is typically much shorter than the circumference. In such situations we may approximate the flow by considering the case when the annular gap is narrow, that is $r_i \approx r_o$ with any variation of pressure in the radial direction negligible with then the radial velocity, v, to be zero [79].

This flow is taken to be composed of a steady axial mean flow denoted by bars and a small perturbations denoted by primes, e.g. $p = \bar{p}(x) + p'(x,\theta,t)$. The disturbances are assumed to have frequency ω in which the temporal dependence is of the form $e^{i\omega t}$. We restrict attention to positive ω without loss of generality. Further, the angular dependence of the perturbations is taken to be of the form $e^{in\theta}$ with circumferential wavenumber n, which we will take to be a non-negative integer. Hence, we consider the disturbances to be of the form $p' = Re[\hat{p}(x)e^{i\omega t + in\theta}]$ etc [111]. Since, $\bar{v} = \bar{w} = 0$ for the uniform mean flow, the solution of the convected wave equation in Eq. (16) is [79,112,113]

$$p'(x,r,t) = (A_+ e^{ik_+ x} + A_- e^{ik_- x})e^{i\omega t + in\theta}, \tag{19}$$

where the axial wavenumbers for the two acoustic waves are

$$\bar{c}k_\pm = \frac{\overline{M}\omega \mp \left[\omega^2 - \omega_{cut-off}^2\right]^{1/2}}{1-\overline{M}^2}, \tag{20}$$

where $\bar{c}$ is the mean speed of sound, $\omega_{cut-off}$ is the cut-off frequency of the duct $(n\bar{c}/r)/(1-\overline{M}^2)^{1/2}$ and $\overline{M}$ is the mean Mach number. When $\omega > \omega_{cut-off}$, A_+ represents a downstream propagating acoustic wave and A_- represents an upstream propagating wave. For $\omega < \omega_{cut-off}$, the term within the square root in Eq. (20) is negative, its square root is a purely imaginary number, and thus the waves have exponential behaviour. Then, k_+ and k_- are chosen such that the $Im(k_+) > 0$ and $Im\ (k_-) < 0$. Then A_+ represents a downstream decaying disturbance and A_- represents an upstream decaying disturbance. The plane wave $n = 0$ propagates at all frequencies.[1] The first circumferential mode propagates

[1] While our analysis for $n > 0$ is for annular combustors, the plane wave case $n = 0$ is relevant for any cross-sectional shape.

at frequencies above $(\bar{c}/r)/(1-\overline{M}^2)^{1/2}$. The exact value of this frequency depends on the mean radius of the annular combustor and the mean temperature and Mach number within it. This is typically in the range of few hundred Hz and is therefore where combustion noise is most important.

Entropy and vortical disturbances convect with the mean flow as shown in Eqs. (17) and (18) and so for disturbances with frequency ω and mode number n, their space–time dependence is $e^{i\omega t+in\theta+ik_0x}$, where $k_0=-\omega/\bar{u}$. The entropy $S=c_v\ \log_e(p/\rho^\gamma)$ and for linear perturbations $S'=c_vp'/\bar{p}-c_p\rho'/\bar{\rho}$. Rearranging this leads to

$$\rho'=\frac{p'}{\bar{c}^2}-\frac{S'\bar{\rho}}{c_p}. \tag{21}$$

We choose to write the constant amplitude of the entropy wave as $A_Ec_p/(\bar{\rho}\bar{c}^2)$, then after substituting for p' from Eq. (19)

$$\rho'=\frac{1}{\bar{c}^2}\left(A_+e^{ik_+x}+A_-e^{ik_-x}-A_Ee^{ik_0x}\right)e^{i\omega t+in\theta}. \tag{22}$$

The velocity perturbations $\vec{u}=(u,0,w)$ can be found from the equation of continuity for linear perturbations

$$i\omega\rho'+\bar{u}\frac{\partial\rho'}{\partial x}+\bar{\rho}\nabla\bullet\vec{u}'=0, \tag{23}$$

or from the momentum equations for the perturbations which become

$$i\omega\bar{\rho}u'+\bar{\rho}\bar{u}\frac{\partial u'}{\partial x}=-\frac{\partial p'}{\partial x}, \tag{24a}$$

$$i\omega\bar{\rho}w'+\bar{\rho}\bar{u}\frac{\partial w'}{\partial x}=-\frac{in}{r}p'. \tag{24b}$$

The contribution to the velocity perturbations from acoustic wave can be calculated easily from Eq. (24):

$$u'=\left(\frac{-k_+}{\bar{\rho}\alpha_+}A_+e^{ik_+x}+\frac{-k_-}{\bar{\rho}\alpha_-}A_-e^{ik_-x}\right)e^{i\omega t+in\theta}, \tag{25a}$$

$$w'=\left(\frac{-n}{r\bar{\rho}\alpha_+}A_+e^{ik_+x}+\frac{-n}{r\bar{\rho}\alpha_-}A_-e^{ik_-x}\right)e^{i\omega t+in\theta}, \tag{25b}$$

where $\alpha_\pm=\omega+\bar{u}k_\pm$. To this we can add any vector that has zero divergence and zero convective derivative, since such a vector will give no contribution to either Eq. (23) or (24). We choose to write this additional vector as

$$u'=\frac{n}{\bar{\rho}\bar{c}}A_Ve^{i\omega t+in\theta+ik_0x}, \tag{26a}$$

$$w'=-\frac{k_0r}{\bar{\rho}\bar{c}}A_Ve^{i\omega t+in\theta+ik_0x}. \tag{26b}$$

The radial component of the velocity needs to be zero to satisfy rigid wall boundary conditions on the wall of the thin annular combustor. The full expression for the velocity perturbations are given from a superposition of Eqs. (25) and (26),

$$u'=\left(\frac{-k_+}{\bar{\rho}\alpha_+}A_+e^{ik_+x}+\frac{-k_-}{\bar{\rho}\alpha_-}A_-e^{ik_-x}+\frac{n}{\bar{\rho}\bar{c}}A_Ve^{ik_0x}\right)e^{i\omega t+in\theta}, \tag{27a}$$

$$w'=\left(\frac{-n}{r\bar{\rho}\alpha_+}A_+e^{ik_+x}+\frac{-n}{r\bar{\rho}\alpha_-}A_-e^{ik_-x}-\frac{k_0r}{\bar{\rho}\bar{c}}A_Ve^{ik_0x}\right)e^{i\omega t+in\theta}. \tag{27b}$$

The strength of vorticity wave can be obtained by substitution for u' and w' from Eq. (27) into the definition of the vorticity, $\vec{\xi}=\nabla\times\vec{u}$. Its radial component is given by

$$\zeta'=(1/r)\partial u'/\partial\theta-\partial w'/\partial x, \tag{28a}$$

and after substitution for u' and w' is found to be equal to

$$\zeta'=\frac{i}{\bar{\rho}\bar{c}r}(n^2+(k_0r)^2)A_Ve^{i\omega t+in\theta+ik_0x}. \tag{28b}$$

In this section we have shown that the perturbations can be expressed as the sum of four waves: two acoustic waves, an entropy wave and a vorticity wave and have the form in Eqs. (19), (22) and (27). The radial velocity component v is zero in this narrow annular gap approximation.

7.2. Analytical solution for the linear waves generated by unsteady combustion

We investigate the perturbations generated in an annular duct by unsteady combustion. For definiteness we will consider the annular geometry introduced in Section 7.1 except that now there is heat input at a flame zone concentrated on $x=0$. The geometry is shown schematically in Fig. 8. Upstream and downstream of the flame zone, linear waves have the form determined in

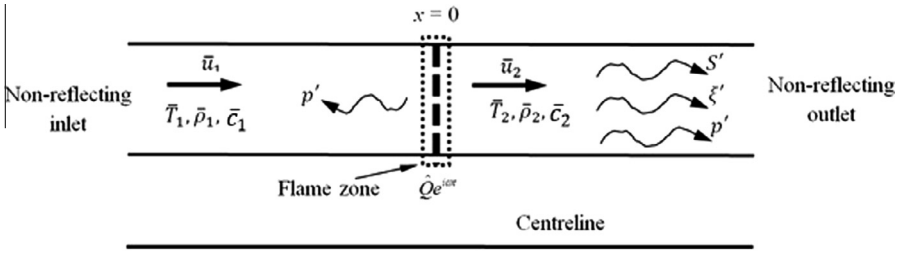

Fig. 8. One-dimensional disturbances in a duct with a mean flow and mean rate of heat release.

Section 7.1. They become coupled across the zone of heat input and their dependence can be found from the equations of conservation of mass, momentum and energy [82,114,115].

An infinite duct is considered with the heat input concentrated at the fixed plane $x = 0$. The energy of flow is increased across $x = 0$ by the rate of heat input, $Q = \overline{Q} + Q'$. The mean heat release rate, $\overline{Q}$, is defined by specifying the value of the mean stagnation temperature after combustion. The linear fluctuations in the rate of heat input have a forced frequency ω and azimuthal mode number n and are denoted by $Q'(t) = \widehat{Q}e^{i\omega t+in\theta}$. No disturbances arrive from upstream nor downstream.

The inlet mean flow is prescribed by setting the pressure, temperature and mass flux. Upstream of the flame region, only an upstream propagating acoustic wave will be present and $S' = \zeta' = 0$. Applying this to Eqs. (19), (22) and (27), the perturbation in flow quantities can be written in the form of

$$p'_1 = A_{-1}e^{ik_{-1}x+i\omega t+in\theta}, \tag{29a}$$

$$\rho'_1 = \frac{1}{\bar{c}_1^2}A_{-1}e^{ik_{-1}x+i\omega t+in\theta}, \tag{29b}$$

$$u'_1 = \frac{-k_{-1}}{\bar{\rho}_1\alpha_{-1}}A_{-1}e^{ik_{-1}x+i\omega t+in\theta}, \tag{29c}$$

$$w'_1 = \frac{-n}{r\bar{\rho}_1\alpha_{-1}}A_{-1}e^{ik_{-1}x+i\omega t+in\theta}, \tag{29d}$$

for $x < 0$. A_{-1} denotes the strength of the acoustic pressure wave.

Downstream of the flame region, there may be convected entropy and vorticity waves in addition to the downstream propagating acoustic wave, and so

$$p'_2 = A_{+2}e^{ik_{+2}x+i\omega t+in\theta}, \tag{30a}$$

$$\rho'_2 = \frac{1}{\bar{c}_2^2}(A_{+2}e^{ik_{+2}x+i\omega t+in\theta} - A_E e^{ik_{02}x+i\omega t+in\theta}), \tag{30b}$$

$$u'_2 = \frac{-k_{+2}}{\bar{\rho}_2\alpha_{+2}}A_{+2}e^{ik_{+2}x+i\omega t+in\theta} + \frac{n}{\bar{\rho}_2\bar{c}_2}A_V e^{ik_{02}x+i\omega t+in\theta}, \tag{30c}$$

$$w'_2 = \frac{-n}{r\bar{\rho}_2\alpha_{+2}}A_{+2}e^{ik_{+2}x+i\omega t+in\theta} + \frac{-k_{02}r}{\bar{\rho}_2\bar{c}_2}A_V e^{ik_{02}x+i\omega t+in\theta}, \tag{30d}$$

for $x > 0$. A_{+2} denotes the strength of the downstream propagating acoustic wave, A_V and A_E are related to the strength of the entropy and vorticity wave respectively, and $k_{02} = -\omega/\bar{u}_2$. The four constants A_{-1},A_{+2},A_E and A_V are related by conservation conditions across the flame zone [82,114,115].

If the heat input is at constant position $x = 0$, then conservation of mass across flame discontinuity is

$$\bar{\rho}_1u'_1 + \rho'_1\bar{u}_1 = \bar{\rho}_2u'_2 + \rho'_2\bar{u}_2, \tag{31a}$$

where the suffices 1 and 2 denote the flow quantities at $x = 0^-$ and $x = 0^+$, respectively.

Conservation of axial momentum across $x = 0$ reveals

$$p'_1 + \rho'_1\bar{u}_1^2 + 2\bar{\rho}_1\bar{u}_1u'_1 = p'_2 + \rho'_2\bar{u}_2^2 + 2\bar{\rho}_2\bar{u}_2u'_2. \tag{31b}$$

Conservation of radial momentum across $x = 0$ is

$$\bar{\rho}_1\bar{u}_1w'_1 = \bar{\rho}_2\bar{u}_2w'_2. \tag{31c}$$

The perturbation in the energy flux out of a control volume around $x = 0$ exceeds the energy flux into it by $Q'(t)$, i.e.

$$c_p\overline{T}_{01}(\bar{\rho}_1u'_1 + \rho'_1\bar{u}_1) + \bar{\rho}_1\bar{u}_1(c_pT'_1 + \bar{u}_1u'_1) + Q'/a = c_p\overline{T}_{02}(\bar{\rho}_2u'_2 + \rho'_2\bar{u}_2) + \bar{\rho}_2\bar{u}_2(c_pT'_2 + \bar{u}_2u'_2), \tag{31d}$$

where $\overline{T}_{01}$ is the mean stagnation temperature, i.e. $\overline{T} + \bar{u}^2/(2c_p)$, and a is the cross-sectional area of the duct. The temperature fluctuation can be related to the pressure and density fluctuation through the perfect gas relationship, $p = R_{gas}\rho T$, which for linear disturbances gives

$$T' = \overline{T}(p'/\bar{p} - \rho'/\bar{\rho}) \tag{32}$$

Equations 31a, 31b and 31d are similar for plane waves, $n = 0$, as presented by Dowling [116]. Equations (31) and (32) can be solved to determine the strength of the waves in terms of the rate of heat input $Q'(t) = \widehat{Q}e^{i\omega t+in\theta}$ but the analysis is tedious. We will give numerical solutions for that in Section 9. Here we concentrate on a low Mach number approximation in which the equations become more tractable.

In the limit $\bar{u}_1, \bar{u}_2 \to 0$, Eq. (31b) simplifies to $p'_1 = p'_2$, and substituting for p'_1 and p'_2 from Eqs. (29a) and (30a) leads directly to

$$A_{-1} = A_{+2} = A, \text{ say.} \tag{33}$$

Equal strength pressure waves are sent upstream and downstream by the unsteady heat release. We have designated the strength of these acoustics waves by the complex amplitude A.

The strength of the vorticity wave then follows directly by substituting for w'_1 and w'_2 from Eqs. (29d) and (30d) into (31c) and using the mean flow conservation of mass flux condition, $\bar{\rho}_1\bar{u}_1 = \bar{\rho}_2\bar{u}_2$. This gives

$$\frac{-n}{r\bar{\rho}_1\alpha_{-1}}A_{-1} = \frac{-n}{r\bar{\rho}_2\alpha_{+2}}A_{+2} + \frac{-k_{02}r}{\bar{\rho}_2\bar{c}_2}A_V. \tag{34a}$$

In the low Mach number limit, $\alpha_+ = \alpha_- = \omega$ and using the definition of $k_{02} = -\omega/\bar{u}_2$ and Eq. (33), we obtain after rearrangement,

$$A_V = \frac{n\bar{c}_2\bar{u}_2}{(r\omega)^2}\left(1 - \frac{\bar{\rho}_2}{\bar{\rho}_1}\right)A. \tag{34b}$$

Since in this low Mach number limit, the combustion takes place at uniform pressure, according to the perfect gas law we have $\bar{\rho}_2/\bar{\rho}_1 = \overline{T}_1/\overline{T}_2$. Also

$\overline{T}_1$ and $\overline{T}_2$ are equal to $\overline{T}_{01}$ and $\overline{T}_{02}$ respectively and so Eq. (34b) can be written as

$$A_V = \frac{n\bar{c}_2\bar{u}_2}{(r\omega)^2}\left(1 - T_R^{-1}\right)A, \tag{34c}$$

where $T_R = \overline{T}_{02}/\overline{T}_{01}$ is the stagnation temperature ratio across the flame.

In a similar way using the equation of conservation of mass across flame (Eq. (31a)) and substituting for u_1', u_2', ρ_1' and ρ_2' from Eqs. (29) and (30) leads to an expression for A_E in terms of A. Some care needs to be taken with the evaluation of the low Mach number limit of $\bar{u}_2\rho_2'$. A first sight it might be thought to be zero but that is incorrect. A_E only enters the jump conditions in Eq. (31) as the product $\bar{u}_2 A_E$. In the limit $\bar{u}_2 \to 0$, $|A_E|$ tends to infinity, in such a way as to keep the product $\bar{u}_2 A_E$ finite. Hence the low Mach number limit of Eq. (31a) is

$$\bar{\rho}_1\left(\frac{-k_{-1}}{\bar{\rho}_1\omega}\right)A = \bar{\rho}_2\left(\frac{-k_{+2}}{\bar{\rho}_2\omega}A + \frac{n}{\bar{c}_2}A_V\right) + \bar{u}_2\left(\frac{-1}{\bar{c}_2^2}\right)A_E. \tag{35a}$$

After substituting for A_V from Eq. (34b), we find that it leads to a term of order Mach number smaller than the other terms which simplify to give

$$A_E = \frac{\bar{c}_2^2}{\bar{u}_2\omega}(-k_{+2} + k_{-1})A. \tag{35b}$$

In the limit $\bar{u} \to 0$, for $\omega > \omega_{cut-off}$, the axial wavenumbers for the two acoustic waves are

$$k_{-1} = \frac{\left[\omega^2 - (\bar{c}_1 n/r)^2\right]^{1/2}}{\bar{c}_1}, \tag{36a}$$

$$k_{+2} = -\frac{\left[\omega^2 - (\bar{c}_2 n/r)^2\right]^{1/2}}{\bar{c}_2}, \tag{36b}$$

while for $\omega < \omega_{cut-off}$, k_{-1} and/or k_{+2} are purely imaginary, the magnitudes of the waves are x dependent and the axial wave numbers for the two acoustic waves are expressed as

$$k_{-1} = -i\frac{\left[(\bar{c}_1 n/r)^2 - \omega^2\right]^{1/2}}{\bar{c}_1}, \tag{36c}$$

$$k_{+2} = +i\frac{\left[(\bar{c}_2 n/r)^2 - \omega^2\right]^{1/2}}{\bar{c}_2}, \tag{36d}$$

where in every case the positive square root is taken of the term in square brackets.

Equations 34c and 35b give the magnitudes of A_V and A_E respectively in terms of A, the magnitude of the pressure waves. Their importance as contributors to indirect and direct sound is determined by their relative contributions to the downstream boundary condition. As discussed in Section 6.1, the appropriate boundary condition for a choked exit is as given by Marble and Candel [12],

$$2\frac{u'}{\bar{u}} + \frac{\rho'}{\bar{\rho}} - \frac{p'}{\bar{p}} = 0. \tag{37a}$$

The terms are to be evaluated in the straight duct just upstream of the nozzle constriction, where the mean flow has been denoted by the suffix 2 and the downstream propagating waves are described in Eq. (30) and produce a reflected upstream propagating reflected acoustic wave whose strength we denote by A_R[2]. After substitution for the waves, in the low Mach number limit, Eq. (37a) gives

$$\frac{2}{\bar{u}_2}\left(\frac{-k_{+2}}{\bar{\rho}_2\alpha_{+2}}Ae^{ik_{+2}L} + \frac{-k_{-2}}{\bar{\rho}_2\alpha_{-2}}A_R e^{ik_{-2}L} + \frac{n}{\bar{\rho}_2\bar{c}_2}A_V e^{ik_{02}L}\right) + \frac{1}{\bar{\rho}_2}\left(\frac{-1}{\bar{c}_2^2}\right)A_E e^{ik_{02}L} = 0, \tag{37b}$$

where the nozzle is considered to be at $x = L$. The ratio of contributions of the direct incident sound wave and the indirect (entropy) noise to the reflected wave A_R is therefore determined by

$$\text{Ratio of direct/indirect (entropy)} = \left|\frac{2k_{+2}\bar{c}_2^2}{\bar{u}_2\alpha_{+2}}\left(\frac{A}{A_E}\right)e^{ik_{+2}L}\right|. \tag{38a}$$

After substitution for A/A_E from Eq. (35b) and using the low Mach number form $\alpha_{+2} = \omega$, we obtain

$$\text{Ratio of direct/indirect (entropy)} = \left|2\left(\frac{k_{+2}}{k_{+2} - k_{-1}}\right)e^{ik_{+2}L}\right|. \tag{38b}$$

For plane waves, $n = 0$, $k_{-1}/k_{+2} = -\bar{c}_2/\bar{c}_1$ and this ratio is independent of frequency and is equal to $2/(1 + \bar{c}_2/\bar{c}_1)$ which is equivalent to $2/(1 + T_R^{1/2})$, where T_R is the mean stagnation temperature ratio across the flame. When there is negligible temperature rise across the flame, the entropy wave contributes as much to the reflected wave as the incident acoustic wave. As the mean temperature increases, the indirect contribution from the entropy wave becomes larger. This ratio is plotted in Fig. 9a. For circumferential waves, the ratio in Eq. (38b) is a function of frequency and mode number as well as mean

[2] In practice, the reflected wave A_R would propagate to the flame zone where it would be partially reflected, subsequently changing strength of the downstream propagating waves. The resultant complex multiply-reflected wave pattern can lead to resonances and is determined numerically in Section 9.3. Here we just consider the first reflection.

temperature ratio. From inspection of k_{-1} and k_{+2}, the ratio depends on frequency only in the combination $\omega r/(n\bar{c}_1)$ and on L in the non-dimensional term Ln/r. At frequencies well below the k_{+2} cut-off, the acoustic wave is exponentially small by the time it reaches the nozzle. The indirect component of the reflected wave is therefore much more substantial than the direct, but this in turn will decay exponentially as it propagates away from the nozzle. The contours of the ratio of the magnitude of direct to indirect (entropy) noise for circumferential modes with $Ln/r = 15$ and 0.5 are plotted in Fig. 9b and c, respectively. For a large value of Ln/r (Fig. 9b), there are two distinct regions for the values of the ratio are visible. For frequencies below the cut-off frequency (based on $\bar{c}_2$), the ratio is very small, effectively zero. While for $\omega > \omega_{cut-off}$, the ratio of direct to indirect noise increases with frequency and asymptotes to the plane wave value $2/(1+T_R^{1/2})$ at high frequencies. The ratio has a maximum magnitude of 1 for $T_R = 1$, indicating that indirect entropy noise is always higher than the direct noise. For a nozzle which is only a short non-dimensional length from the combustion region, $Ln/r = 0.5$, Fig. 9c shows three different regions for the ratio of the magnitude of direct to indirect (entropy) noise. For frequencies $\omega > \omega_{cut-off}$ (based on $\bar{c}_2$) the ratio in Fig. 9c behaves like that in Fig. 9b and asymptotes to the plane wave value at high frequencies. At the cut-off frequency based on $\bar{c}_2, k_{+2} = 0$ and it is evident from Eq. (38b) that the contribution from the direct sound wave vanishes. The zero along $\omega r/(n\bar{c}_1) = T_R^{1/2}$ is clearly seen in Fig. 9c. However, for frequencies just below the cut-off frequency, even though k_{+2} is imaginary the decay due to the exponential $e^{ik_{+2}L}$ is modest, because the non-dimensional length Ln/r is small. Hence the magnitude of the ratio is dominated by the value of the fraction $|2k_{+2}/k_{+2} - k_{-2}|$ in Eq. (38b) and this has a maximum value of 2 when $\omega r/(n\bar{c}_1) = 1$. This local maximum for each T_R is seen clearly in Fig. 9c. As the frequency decreases further, both k_{-1} and k_{+2} are purely imaginary and of opposite sign and so $|2k_{+2}/k_{+2} - k_{-2}|$ gradually decreases.

The relative contribution of the vorticity wave can be determined in a similar way and is described by

$$\text{Magnitude of ratio of direct/indirect (vorticity)} = \left|\frac{k_{+2}\bar{c}_2}{n\alpha_{+2}}\left(\frac{A}{A_V}\right)e^{ik_{+2}L}\right|, \tag{39a}$$

which, after substituting for A/A_V from Eq. (34c) leads to

$$\text{Ratio of direct/indirect (vorticity)} = \left|\left(\frac{\omega r}{n\bar{c}_2}\right)^2\frac{\bar{c}_2 k_{+2}}{\omega\overline{M}_2}\left(1-T_R^{-1}\right)^{-1}e^{ik_{+2}L}\right|. \tag{39b}$$

Because this involves division by the mean flow Mach number $\overline{M}_2$, this ratio is large in the low Mach number limit and the vorticity wave is not an important contributor to indirect noise.

7.2.1. Solution for the acoustic wave

The solution for the acoustic wave strength A in terms of the unsteady rate of heat input $Q'(t) = \widehat{Q}e^{i\omega t+in\theta}$ follows from substituting for A_E and A_V from Eqs. (35b) and (34c) into the equation of conservation of energy across the flame zone, Eq. (31d). It is convenient to begin an investigation of low mean flow Mach numbers by noting that Eq. (31a) may be used to recast the energy Eq. (31d) in the form:

$$\bar{\rho}_2\bar{u}_2\left(c_pT_2' + \bar{u}_2u_2'\right) = Q'/a - c_p(\overline{T}_{02} - \overline{T}_{01})\left(\bar{\rho}_1u_1' + \rho_1'\bar{u}_1\right) + \bar{\rho}_1\bar{u}_1\left(c_pT_1' + \bar{u}_1u_1'\right). \tag{40}$$

All the terms involving multiplication of the mean flow velocity can be neglected in the low Mach number approximation except the term $\bar{\rho}_2\bar{u}_2c_pT_2'$. T_2' includes a contribution from the entropy wave described by A_E which tends to infinity as $\bar{u}_2 \to 0$ in such a way as to keep $\bar{u}_2T_2'$ finite. We evaluate $\bar{u}_2T_2'$ by first using the linearized form of the perfect gas equation in Eq. (32), $T' = \overline{T}(p'/\bar{p} - \rho'/\bar{\rho})$, and then substituting for ρ_2' from Eq. (30b). In the low Mach number limit this simplifies to

$$\bar{\rho}_2\bar{u}_2c_pT_2' = \frac{\bar{u}_2c_p\overline{T}_2}{\bar{c}_2^2}A_Ee^{ik_{02}x+i\omega t+in\theta} = \frac{\bar{u}_2}{(\gamma-1)}A_Ee^{ik_{02}x+i\omega t+in\theta}. \tag{41a}$$

After substituting this form for $\bar{\rho}_2\bar{u}_2c_pT_2'$ into Eq. (40) and using the form for u_1' in Eq. (29c) we obtain,

$$\frac{\bar{u}_2}{(\gamma-1)}A_E = \frac{\widehat{Q}}{a} - c_p(\overline{T}_{02} - \overline{T}_{01})\left(\frac{-k_{-1}}{\alpha_{-1}}\right)A. \tag{41b}$$

Substituting for A_E from Eq. (35b) finally gives

$$\left|\frac{A}{\widehat{Q}}\right| = \frac{1}{a}\frac{\gamma-1}{\bar{c}_1^2}T_R^{-1}\left|\frac{\omega}{-k_{+2}+T_R^{-1}k_{-1}}\right|, \tag{42a}$$

so that

$$\left|\frac{\hat{p}}{\widehat{Q}}\right| = \frac{1}{a}\frac{\gamma-1}{\bar{c}_1^2}T_R^{-1}\left|\frac{\omega}{-k_{+2}+T_R^{-1}k_{-1}}e^{ik_{+2}x}\right|, \tag{42b}$$

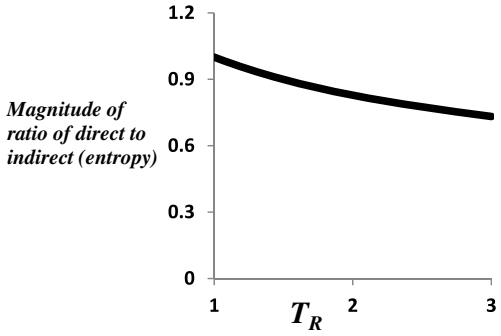

(a) $n = 0$

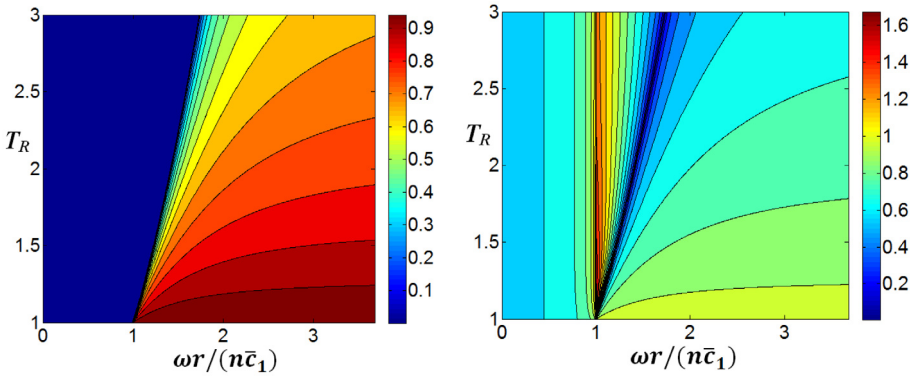

(b) $Ln/r = 15$ (c) $Ln/r = 0.5$

Fig. 9. Ratio of the magnitude of direct acoustic to indirect (entropy) noise as a function of temperature ratio and frequency obtained using Eq. (38b) for (a) plane wave with $n = 0$, and for circumferential waves with Ln/r equal to (b) 15 and (c) 0.5.

where k_{+2} and k_{-1} are presented in Eqs. (36a)–(36d). For $\omega < \omega_{cut-off}$, k_{+2} and/or k_{-1} are purely imaginary and hence the acoustic waves are decay along the duct, and hence the wave amplitudes are x dependent. For $\omega > \omega_{cut-off}$, the magnitude of transfer function of acoustic wave to the unsteady rate of heat addition is independent of x and is obtained as

$$\left|\frac{\hat{p}}{\hat{Q}}\right| = \frac{1}{a}\frac{\gamma-1}{\bar{c}_1^2}T_R^{-1}\left|\frac{\omega}{-k_{+2}+T_R^{-1}k_{-1}}\right|. \tag{42c}$$

For plane waves ($n = 0$), Eq. (42c) is simplified as

$$\left|\frac{\hat{p}}{\hat{Q}}\right|_{n=0} = \frac{\gamma-1}{a\bar{c}_1}\frac{1}{1+T_R^{1/2}}, \tag{42d}$$

an expression that is independent of frequency. Equation (42d) shows that in the case of negligible mean heat release when $\overline{T}_{02} = \overline{T}_{01}$ and $T_R = 1$, the magnitude of the transfer function (the magnitude of the ratio of the pressure perturbation to the fluctuation in heat release rate that generated it) tends to $(\gamma-1)/(2a\bar{c}_1)$. Further, it shows that as temperature ratio across the flame increases the magnitude of the transfer function wave decreases.

7.2.2. Solution for the entropy wave

The amplitude A_E was defined such that the entropy fluctuation is given by

$$\hat{S} = \frac{c_p}{\bar{\rho}_2\bar{c}_2^2}A_E e^{ik_0 x}. \tag{43}$$

Substituting for A_E and A presented in Eq. (35b) into Eq. (42d) results in

$$\left|\frac{\hat{S}}{\hat{Q}}\right| = \frac{1}{\bar{m}}T_R^{-1}\left|1+\frac{(1-T_R^{-1})k_{-1}}{-k_{+2}+T_R^{-1}k_{-1}}\right|, \tag{44a}$$

using $c_p/R = \gamma/(\gamma-1)$, $\bar{c}_1^2 = \gamma R\overline{T}_{01}$ and mass flow rate $m = \rho_1 u_1 a$ has been introduced. Since the entropic waves convect with the mean flow, Eq. (44a) holds for all frequencies ω whether below or above $\omega_{cut-off}$.

The result in Eq. (44a) can be interpreted by expanding $c_p T_2'$ and substituting for $\overline{Q}/\bar{m} = c_p(\overline{T}_{02}$

$-\overline{T}_{01}$) and $m'/a = \bar{\rho}_1 u'_1 + \rho'_1 \bar{u}_1$ into Eq. (40) which leads to

$$\frac{\bar{\rho}_2 \bar{u}_2 \bar{c}_2^2 a}{(\gamma-1)c_p} S' = Q' - \overline{Q}\frac{m'}{\bar{m}}. \tag{44b}$$

In this form it is clear that the entropy wave is generated by fluctuations in Q/m, the rate of heat released/mass flow rate. Even if the fluctuation in the rate of heat release is zero, i.e. $Q'(t) = 0$, fluctuations in inlet mass flow m' will still generate entropy fluctuations if the mean rate of heat release $\overline{Q}$ is nonzero.

Equation (44a) shows that as $T_R = \overline{T}_{02}/\overline{T}_{01} \to 1$, the magnitude of the entropy wave transfer function $\widehat{S}/\widehat{Q}$ tends to $\bar{m}^{-1}$. As we predicted in Section 7.2, Eq. (44a) shows that in the limit $\bar{u} \to 0, \bar{m} \to 0$ the strength of the entropy wave $|\widehat{S}|$ tends to infinity. However, $\bar{m}S$ remains finite. So when comparing results for varying Mach numbers in Section 9, it is convenient to plot $(\widehat{S}/c_v)/(\widehat{Q}/\overline{Q})$, where c_v is the specific heat at constant volume and $\overline{Q}$ is the mean heat release rate as $\bar{m}c_p(\overline{T}_{02} - \overline{T}_{01})$. It follows directly from Eq. (44a) that

$$\left|\frac{\widehat{S}/c_v}{\widehat{Q}/\overline{Q}}\right| = \gamma(1 - T_R^{-1})\left|1 + \frac{(1-T_R^{-1})k_{-1}}{-k_{+2} + T_R^{-1}k_{-1}}\right|. \tag{44c}$$

For plane waves ($n = 0$), Eq. (44c) simplifies to

$$\left|\frac{\widehat{S}/c_v}{\widehat{Q}/\overline{Q}}\right|_{n=0} = \gamma\left(T_R^{1/2} - T_R^{-1/2}\right). \tag{44d}$$

Equation (44d) clearly shows that, similar to the acoustic waves, the magnitude of the entropy wave transfer function for plane waves is independent of the frequency.

It should be pointed out that while the results in Eqs. (44a) and (44c) always apply just downstream on the flame zone, they can only be applied at large x if the dissipation of entropy wave is negligible. In a low Mach number flow the wavelength of the entropy wave, $2\pi\bar{u}_2/\omega$, is very short indeed for high-frequency disturbances [5]. Then turbulent mixing and diffusion tend to smooth out the entropy fluctuations as they convect downstream. As a consequence, although a strong entropy fluctuation may be generated in the flame zone, the amplitude of a high frequency entropic disturbance may be negligible by the time the wave reaches the exit of the combustor. Judgment is needed, based on the ratio of mixing to convection time, to decide whether the entropy waves persist as far as any downstream contraction. If they do not, ρ' should be replaced by its acoustic contribution $p'/\bar{c}^2$ in Eq. (30b) far downstream of the flame zone. We would expect the entropy fluctuations to only be important at combustor exit for mid to low frequencies [5].

7.2.3. Solution for the vorticity wave

In this section, we investigate the flow physics involved in the generation of the vorticity wave and determine the wave strength analytically. Using Eq. (28b) and knowing that in the low Mach number limit n^2 is negligible compared to $(k_{02}r)^2$, the vorticity wave is obtained as

$$\zeta' = \frac{i}{\bar{\rho}_2 \bar{c}_2} k_{02}^2 r A_V e^{i\omega t + in\theta + ik_{02}x}. \tag{45}$$

Substituting for A_V from Eq. (34c) into Eq. (45) results in

$$\zeta' = \frac{-in}{r\bar{\rho}_1\bar{u}_2}\left(1 - \frac{\bar{\rho}_1}{\bar{\rho}_2}\right) A e^{i\omega t + in\theta + ik_{02}x}. \tag{46a}$$

Since $\bar{\rho}_2\bar{u}_2 = \bar{\rho}_1\bar{u}_1$, after some rearrangement Eq. (46a) leads to

$$\zeta' = \frac{-1}{r\bar{u}_1} \times \frac{1}{\bar{\rho}_1^2}(\bar{\rho}_2 - \bar{\rho}_1) \times inAe^{i\omega t + ik_{02}x + in\theta}. \tag{46b}$$

Knowing that $\partial p'/\partial\theta = in\, Ae^{i\omega t\, + in\theta}$ and substituting for $inAe^{i\omega t + in\theta}$ in Eq. (46b) gives

$$\zeta' = \left(\frac{-1}{\bar{u}_1\bar{\rho}_1^2}\right) \times (\bar{\rho}_2 - \bar{\rho}_1) \times \left[\frac{1}{r}\frac{\partial p'}{\partial\theta}\right] \text{ on } x = 0. \tag{46c}$$

Equation (46c) demonstrates that $\zeta' \propto (\bar{\rho}_2 - \bar{\rho}_1) \times (\frac{1}{r}\frac{\partial p}{\partial\theta})$: the vorticity generated at the flame on $x = 0$ is due to the baroclinic ($\nabla p \times \nabla\rho$) vorticity production mechanism [117], involving the gradient of the mean density across the flame and the gradient of acoustic pressure fluctuation in the circumferential direction.

The magnitude of the vorticity wave can be obtained by substituting for A from Eq. (42a) and using $k_{02} = -\omega/\bar{u}_2, \bar{u}_2 = \bar{m}/(\bar{\rho}_2 a) = \bar{m}\overline{T}_{02}/(\overline{T}_{01}\bar{\rho}_1 a), \bar{c}_2 = \bar{c}_1(\overline{T}_{02}/\overline{T}_{01})^{1/2}$. This gives

$$\frac{\hat{\zeta}}{\widehat{Q}} = \frac{n(\gamma-1)}{\bar{m}r\bar{c}_1^2}\left(1 - T_R^{-1}\right)T_R^{-1} \times \frac{\omega}{-k_{+2} + T_R^{-1}k_{-1}} ie^{ik_{02}x}. \tag{47a}$$

The magnitude of transfer function for the vorticity wave is expressed as

$$\left|\frac{\hat{\zeta}}{\widehat{Q}}\right| = \frac{n(\gamma-1)}{\bar{m}r\bar{c}_1^2}(1 - T_R^{-1})T_R^{-1}\left|\frac{\omega}{-k_{+2} + T_R^{-1}k_{-1}}\right|. \tag{47b}$$

Just as for the entropy waves, since the vorticity waves convect with the mean flow, Eq. (47b) holds for all frequencies ω whether they are below or above $\omega_{cut-off}$. Furthermore, this equation shows that magnitude of the vorticity transfer function has the same variation with frequency above $\omega_{cut-off}$ as that for the pressure wave presented in Eq. (42b).

It is seen that in the case of no mean heat release, $\overline{T}_{02} = \overline{T}_{01}, T_R = 1$, the magnitude of the vorticity perturbation is zero. The explanation is simple. Then there is no change in the mean density across the flame. Therefore, according to the baroclinic vorticity production mechanism in Eq. (46c), the amount of vorticity produced is zero. It is also clear from Eq. (47b) that for the plane wave ($n = 0$) there is no vorticity generation and hence $|\hat{\zeta}/\widehat{Q}| = 0$. In this case the circumferential pressure gradient is zero.

Equation (47b) shows that at fixed frequency and T_R, the transfer function of the vorticity wave $|\hat{\zeta}/\widehat{Q}|$ is proportional to $\bar{m}^{-1}$ and so tends to infinity in the limit $\bar{u} \to 0$. Of course in practice $|\widehat{Q}|$ tends to zero if it is proportional to $\overline{Q}$ because the oncoming mean velocity tends to zero. Hence in the numerical results in Section 9 we chose to represent the transfer function for vorticity wave in terms of $|\hat{\zeta}/(\widehat{Q}/\overline{Q})|$, which is given by

$$\left|\frac{\hat{\zeta}}{\widehat{Q}/\overline{Q}}\right| = \frac{n}{r}\left(1 - T_R^{-1}\right)^2 \left|\frac{\omega}{-k_{+2} + T_R^{-1}k_{-1}}\right|. \tag{48}$$

8. Numerical results

The main application of high-fidelity numerical methods is to enhance the understanding of the fundamental physical processes. In real industrial design environments there is an additional need for less computational time intensive prediction tools that can be used before the full geometry has been defined and that are sufficiently quick to be useable for design optimisation. This is particularly important for noise generation and transmission because the regions through which acoustic waves propagate are extensive requiring large computational domains. Therefore, low-order models are required. These tools provide the fastest approach for the design and optimisation of combustors and combustor-turbine coupling. A computer program LOTAN (Low-Order Thermo-Acoustic Network model) is one such low-order model. It calculates numerically the linear waves (acoustic, entropic and vortical) generated by unsteady heat input in a complicated network of pipes provided suitable boundary conditions are applied. The program is intended for circular or thin annular combustors, typical of aeroengines, so axial and circumferential variations are included but radial dependence is ignored. This thermoacoustic network model was developed to predict combustion instabilities. If a flame model is prescribed to relate unsteady combustion to flow perturbations, the code can be used to obtain the frequencies of the resonant modes, their stability and mode shapes. It models plane wave and circumferential modes of combustion instabilities [5,7,79,118]. Alternatively, LOTAN can be used to determine the forced response to specified unsteady heat input at frequency ω and circumferential mode number n [4]. We will use LOTAN to investigate the linear waves generated by unsteady heat release in the geometry introduced for the analytical study in Section 7. There the solutions obtained were for low mean flow Mach numbers. Using LOTAN we can also investigate the variation with Mach number. The results are described in terms of transfer functions $|\hat{p}/\widehat{Q}|, |\widehat{S}/c_v|/|\widehat{Q}/\overline{Q}|$ and $|\hat{\zeta}|/|\widehat{Q}/\overline{Q}|$ which describe the flow response to unsteady heat input of unit amplitude at frequency ω and circumferential mode number n.

8.1. Description of the model

The model used in the LOTAN program assumes that the flow is composed of a steady axial mean flow and small amplitude perturbations. The mean flow is assumed to be one-dimensional and the perturbations vary axially and circumferentially but are independent of radius. The model is formulated in terms of a network of modules describing the features of the geometry. For duct modules of constant cross-sectional area and no heat input, acoustic wave propagation and convection of entropy and vorticity waves are used to relate the perturbations at one end of the duct to those at the other. Quasi-steady conservation laws for mass, momentum and energy are used to relate flow perturbations across zones of heat input and across duct junctions. The application of inlet and outlet boundary conditions then enables determination of the linear perturbations. A perfect gas is assumed and the specific heats of c_p,c_v and γ are assumed to be temperature dependent as $c_p(T) = 973.6 + 0.1333 \times T$, where T is in (K) and c_p is in J/kg K [111,118,119].

8.2. Formulation

Combining the expressions for the four waves presented in Section 7 we have

$$(\hat{p}, \hat{\rho}, \hat{u}, \hat{w})^{\mathrm{T}} = \mathbf{F}\vec{W}(x), \tag{49a}$$

where

$$\vec{W}(x) = \left(A_+ e^{ik_+ x},\ A_- e^{ik_- x},\ A_E e^{ik_0 x},\ A_V e^{ik_0 x}\right)^{\mathrm{T}}, \tag{49b}$$

$$\mathbf{F} = \begin{pmatrix} 1 & 1 & 0 & 0 \\ \frac{1}{\bar{c}^2} & \frac{1}{\bar{c}^2} & -\frac{1}{\bar{c}^2} & 0 \\ \frac{-k_+}{\bar{\rho}\alpha_+} & \frac{-k_-}{\bar{\rho}\alpha_-} & 0 & \frac{n}{\bar{\rho}\bar{c}} \\ \frac{-n}{r\bar{\rho}\alpha_+} & \frac{-n}{r\bar{\rho}\alpha_-} & 0 & \frac{-k_0 r}{\bar{\rho}\bar{c}} \end{pmatrix}. \tag{49c}$$

At the flame discontinuity the jump conditions are satisfied by conserving the mass flux, $m = \rho ua$, axial momentum flux, $f_x = pa + mu$ and radial momentum flux, $f_\theta = rmw$. Across the flame or

zone of heat input the energy flux, $e = mc_p T + m(u^2 + w^2)/2 = a\gamma pu/(\gamma - 1) + m(u^2 + w^2)/2$, increases due to the rate of addition of heat. The perturbations of these fluxes are given by [111,119]

$$(\hat{m}, \hat{f}_x, \hat{f}_\theta, \hat{e})^{\mathrm{T}} = \mathbf{G}(\hat{p}, \hat{\rho}, \hat{u}, \hat{w})^{\mathrm{T}}, \tag{49d}$$

where

$$\mathbf{G} = a\begin{pmatrix} 0 & \bar{u} & \bar{\rho} & 0 \\ 1 & \bar{u}^2 & 2\bar{\rho}\bar{u} & 0 \\ 0 & 0 & 0 & r\bar{\rho}\bar{u} \\ \frac{\gamma\bar{u}}{\gamma-1} & \frac{1}{2}\bar{u}^3 & \frac{\gamma\bar{p}}{\gamma-1} + \frac{3}{2}\bar{\rho}\bar{u}^2 & 0 \end{pmatrix}. \tag{49e}$$

Using the matrices **F** and **G** we can easily convert between wave amplitudes, flow perturbations and flux perturbations. Given $\hat{p}, \hat{\rho}, \hat{u}$ and $\hat{w}$ at the start of the duct we can find $\vec{W}(x_0)$ (where x_0 is the start of the duct) by inverting Eq. (49a). The wave amplitudes at the end of the duct ($x = x_{0+}L$) are then $\vec{W}(x_0 + L) = \mathbf{P}(L)\vec{W}(x_0)$ where $\mathbf{P}(L)$ is the propagation matrix,

$$\mathbf{P}(L) = \begin{pmatrix} e^{ik_+L} & 0 & 0 & 0 \\ 0 & e^{ik_-L} & 0 & 0 \\ 0 & 0 & e^{ik_0L} & 0 \\ 0 & 0 & 0 & e^{ik_0L} \end{pmatrix}. \tag{49f}$$

We will also require the perturbations in entropy and vorticity that are determined using Eqs. (21) and (28b), respectively [111,119].

8.3. Boundary conditions

At the inlet the mean flow is prescribed by setting the pressure, temperature and mass flux. The perturbations are given by the type of inlet. For a semi-infinite inlet pipe only an upstream propagating acoustic wave will be present and so we take, $A_+ = A_E = A_V = 0$ and A_- will be calculated as part of the solution. At the outlet ($x = L$) there is a boundary condition on flow perturbations. For a semi-infinite outlet pipe, the boundary condition is that there is no upstream wave, $A_- = 0$ [111,119].

For the second part of the results presented in Section 9.3 for a nozzle, the outlet boundary is considered to be choked, which is a good approximation for the turbine inlet, and the nozzle is assumed to be sufficiently short to be treated as compact. Then for $n = 0$, the boundary condition found by Marble and Candel [12] gives

$$2\frac{\hat{u}}{\bar{u}} + \frac{\hat{\rho}}{\bar{\rho}} - \frac{\hat{p}}{\bar{p}} = 0. \tag{50}$$

Using the Euler equations for a narrow annular gap, Stow et al. [79] have shown that the boundary condition found by Marble and Candel [12] also applies for circumferential modes provided the nozzle is compact.

9. Results

In this section the results of the analytical expressions presented in Section 7 and the numerical results obtained using LOTAN described in Section 8 are compared. First the errors introduced by the approximation of neglecting the mean flow Mach number presented in Section 7 are investigated. Then the numerical results for amplitudes of acoustic, entropy and vorticity waves are presented as functions of frequency, Mach number and temperature ratio across the flame. The geometry considered in the numerical simulation is summarized in Table 1 and we consider the inlet stagnation pressure and stagnation temperature to be 12 bar and 653 K respectively.

9.1. Validation of zero mean flow approximation

In this section, the analytical results of Section 7 are compared with numerical results from LOTAN obtained at the duct outlet ($x = L$) to investigate the range of validity of the low-Mach number approximation. With the conditions summarized in Table 1, LOTAN calculations are performed for a wide range of forced frequencies, $f = \omega/2\pi$, from $f = 200 - 1200$ Hz, temperature ratio across the flame $T_R = \overline{T}_{02}/\overline{T}_{01}$ from 1.1 to 5 and two different inlet Mach numbers, $\overline{M}_{01} = 0.06$ and $\overline{M}_{01} = 0.1$. The specific heats are assumed to be temperature dependent. However, to aid comparison with analytical results, the numerical computation is also performed with uniform specific heats that is computed as $c_p(T_{average}) = 973.6 + 0.1333 \times (\overline{T}_{02} + \overline{T}_{01})/2$, where T is in (K) and c_p is in J/kg K.

Figure 10 shows the wave amplitudes obtained by the analytical solution and LOTAN with uniform c_p, and LOTAN with temperature dependent c_p as a function of frequency for $\overline{M}_{01} = 0.06, \overline{T}_{02}/\overline{T}_{01} = 3.0$ and $n = 1$ with a non-reflective downstream boundary condition. The results are presented for a distance L downstream of the combustion zone. The peak observed in the amplitude of the three waves corresponds to the cut-off frequency based on the sound speed downstream of the flame, i.e. $\omega_{cut-off}/2\pi \approx 460$ Hz. The acoustic, entropic and vortical transfer functions obtained analytically are in very good agreement

Table 1
Summary of the geometry.

Axial position of the flame, $x = 0.0$
Mean radius of duct, $r = 0.3$ m
Total cross-sectional area, $a = 0.3$ m^2
Distance between the flame and the outlet, $L = 0.5$ m

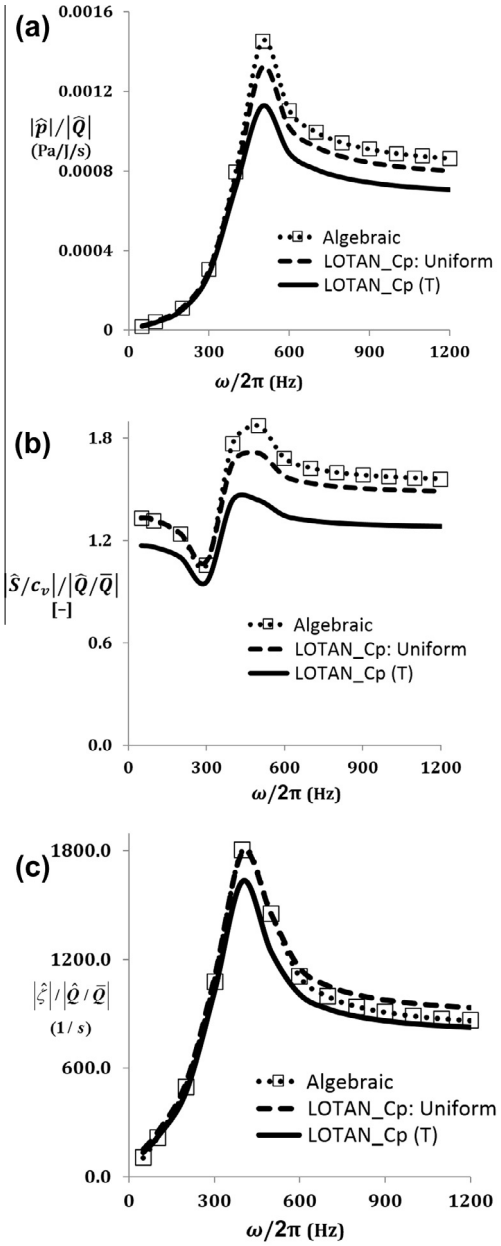

Fig. 10. Comparison between analytical solutions based on low Mach number mean flow approximation (dashed line with symbol) obtained using Eqs. (42b), (44c) and (48) with LOTAN for uniform c_p (dashed line) and LOTAN with temperature dependent c_p (solid line), as a function of frequency, $\omega/2\pi$, for $\overline{T}_{02}/\overline{T}_{01} = 3.0$, $\overline{M}_{01} = 0.06$ and for the first circumferential mode $n = 1$ at the non-reflecting duct outlet $x = L$.

with the results of LOTAN with uniform c_p, the difference in general being less than the error from neglecting the variation c_p with temperature. Therefore, the low mean flow Mach number approximation captures reasonably well the main characteristics of the wave transfer functions, including their general behavior as a function of frequency. In addition, the results presented in Fig. 10 clearly show the effect of specific heat variations on the transfer functions. For example at high temperature ratios there is up to 15% difference between the results for uniform c_p compared with those for a temperature dependent c_p.

The validity of low the Mach number approximation is tested as a function of temperature ratio for a fixed frequency of $\omega/2\pi = 200$ Hz and circumferential mode number $n = 1$. This frequency is below the cut-off frequencies based on the sound speeds downstream of the flame that change between 300 Hz-600 Hz for the range of temperature ratios considered. Results for the amplitudes of the transfer functions for the different waves are shown in Fig. 11 for a mean flow Mach number of $\overline{M}_{01} = 0.06$ and Fig. 12, for $\overline{M}_{01} = 0.10$. It is seen that for all three waves and both Mach numbers, the results obtained using the low mean Mach number approximation are in excellent agreement with the results of LOTAN with uniform specific heat for modest temperature ratios. The maximum error is for the vorticity wave at the higher Mach number and highest temperature ratio where the error is about 20%. However, since $\overline{M}_{02} = \overline{M}_{01} T_R^{1/2}$, at those conditions the downstream Mach number is about 0.22, stretching the limit of the low Mach number approximation where we neglect terms of order $\overline{M}$ in comparison with unity. Comparing Figs. 11 and 12 shows that the transfer functions are only weakly influenced by the mean inlet Mach number and that the normalization we chose for the wave amplitudes (i.e. dividing the entropy and vorticity wave amplitudes by $\widehat{Q}/\overline{Q}$) captures much of the variation with Mach number.

Generally speaking the results presented in this section show that for a practical range of frequencies (few hundred Hz) and low temperature ratios ($\overline{T}_{02}/\overline{T}_{01} \approx 2$ to 3) the results obtained based on the low Mach number approximation are in excellent agreement with LOTAN. Therefore, the low mean flow approximation captures reasonably well the main characteristics of the acoustic, entropy and vorticity waves. Nonetheless, for high frequencies and high temperature ratios the results show that the low mean flow approximation may lead to error in determining the strength of the three waves and then a computation of the linearized Euler equations (LEE) as provided, for example, by LOTAN is required.

9.2. Characteristics of the waves

Downstream of the heat release zone, the downstream-travelling/attenuating acoustic wave, the entropy and vorticity waves generated by the

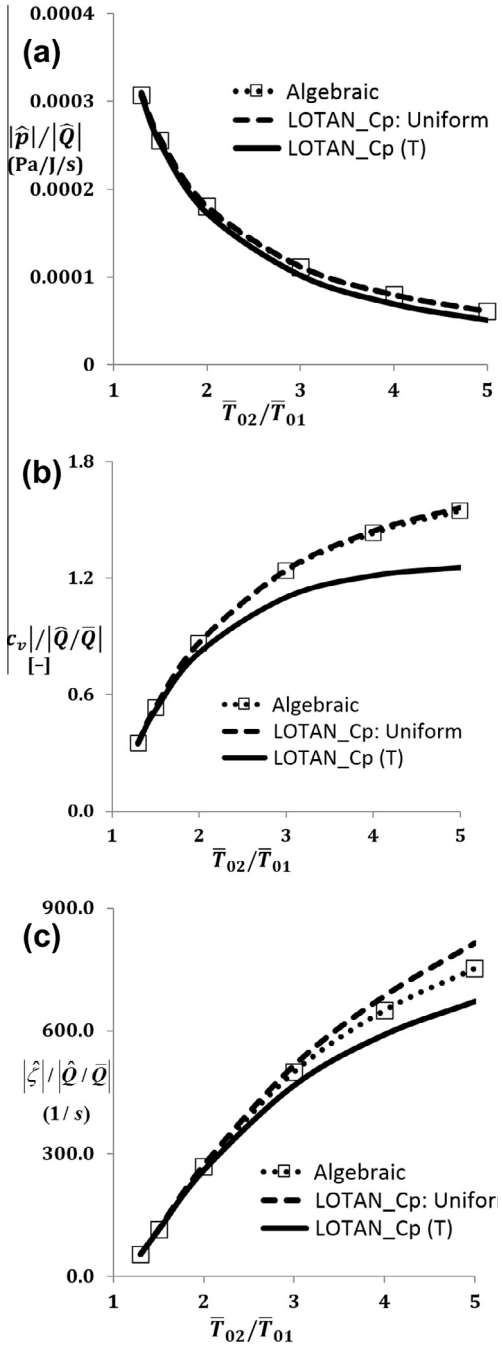

Fig. 11. Comparison between analytical solutions based on zero mean flow approximation (dashed line with symbol) obtained using Eqs. (42b), (44c) and (48) with LOTAN for uniform c_p (dashed line) and LOTAN with temperature dependent c_p (solid line), as a function of $\overline{T}_{02}/\overline{T}_{01}$, for $f = 200$ Hz, $\overline{M}_{01} = 0.06$ and for the first circumferential mode $n = 1$ at the non-reflecting duct outlet $x = L$.

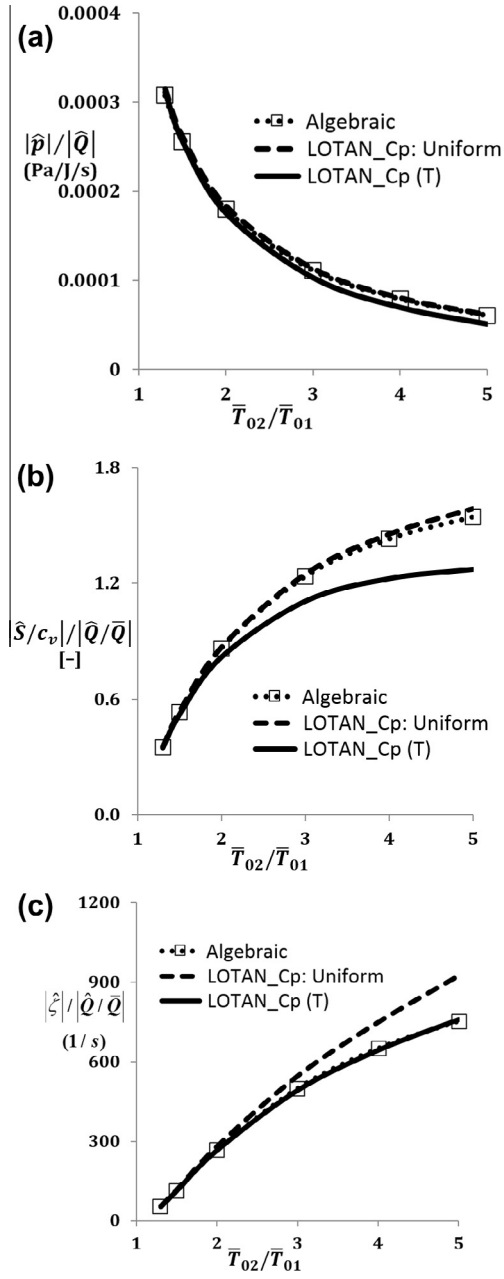

Fig. 12. Comparison between analytical solutions based on zero mean flow approximation (dashed line with symbol) obtained using Eqs. (42b), (44c) and (48) with LOTAN for uniform c_p (dashed line) and LOTAN with temperature dependent c_p (solid line), as a function of $\overline{T}_{02}/\overline{T}_{01}$, for $f = 200$Hz, $\overline{M}_{01} = 0.1$ and for the first circumferential mode $n = 1$ at the non-reflecting duct outlet $x = L$.

unsteady combustion move towards the duct exit. Results are presented first for a non-reflecting downstream boundary. We will investigate the characteristics of the three waves for circumferential wave numbers, $n = 0, 1, 2$ by running LOTAN

for temperature dependent specific heats and investigate the effects of frequency, temperature ratio and inlet Mach number. In the previous section, we demonstrated the usefulness of the low Mach number analytical solution and this will be used to interpret the numerical results.

9.2.1. Effect of inlet Mach number

To study further the effects of a non-negligible mean flow Mach number, the numerical calculations are performed for a wide range of inlet Mach numbers and three circumferential wave numbers, $n = 0, 1, 2$. The magnitude of the acoustic, entropy and vorticity waves at the duct outlet ($x = L$) are shown for a temperature ratio of $\overline{T}_{02}/\overline{T}_{01} = 3$ and frequency of $\omega/2\pi = 200$ Hz in Fig. 13. It is seen that, with the normalization we have chosen, the magnitudes of the transfer functions for the acoustic, entropy and vorticity waves tend to finite non-zero numbers showing that our choice of normalization (i.e. dividing the entropy and vorticity wave strength by $\widehat{Q}/\overline{Q}$) has been appropriate to capture the variation with Mach number at low Mach numbers. Figure 13a shows that for plane waves, $n = 0$, as the Mach number increases the magnitude of the acoustic wave decreases. The difference between the magnitudes of the acoustic waves obtained for the higher mean Mach numbers compared with the low Mach number asymptote is about 25%. The same difference also occurs at higher circumferential mode numbers and is consistent with terms of order Mach number being neglected in comparison with unity in the low Mach number asymptotic form. For higher circumferential wavenumbers, the frequency of 200 Hz is below the cut-off frequency and the magnitude of the acoustic wave at a distance downstream of the zone of combustion is exponentially small. For instance when $n = 2$ the magnitude of the acoustic wave at the duct exit is $|\hat{p}|/|\widehat{Q}| = 7.0 \times 10^{-6}$ Pa J^{-1}s in the low Mach number limit.

Figure 13b and c show the effect of the inlet Mach numbers on the entropy and vorticity waves respectively. Figure 13b shows that similar to the acoustic wave, although for the plane waves the magnitude of the entropy waves decreases with an increase of mean Mach number, the difference between the maximum and minimum values of $|\widehat{S}/c_v|/|\widehat{Q}/\overline{Q}|$ is less than 10%. The variation of inlet Mach number has more influence on the magnitude of the vorticity wave than on the acoustic and entropic waves. Nonetheless, it is seen that for $\overline{M}_{01} < 0.1$, the magnitude of the vorticity wave is almost independent of the value of $\overline{M}_{01}$.

9.2.2. Effect of frequency

In this section the effect of the frequency of the heat release rate fluctuation on the amplitudes of the acoustic, entropy and vorticity waves is studied computationally for an inlet Mach number $\overline{M}_{01} = 0.06$ and $\overline{T}_{02}/\overline{T}_{01} = 3$. For frequencies below cut-off, $\omega_{cut-off}/2\pi$ (~460 Hz and

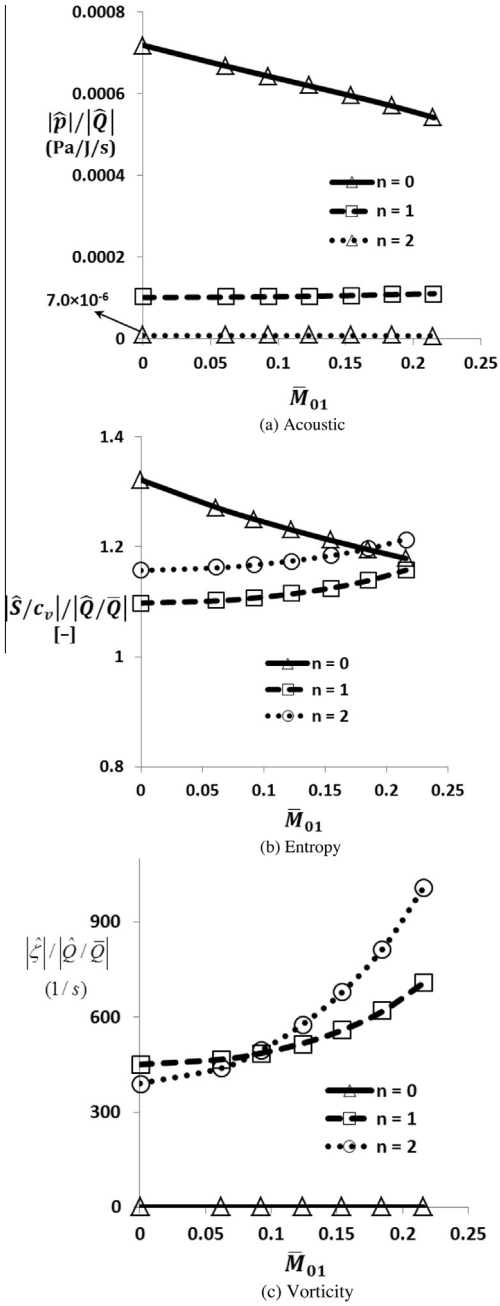

Fig. 13. Magnitude of three waves as a function of inlet Mach number obtained for a frequency of 200 Hz and $\overline{T}_{02}/\overline{T}_{01} = 3$, for circumferential wave numbers $n = 0$ (solid line with triangles), $n = 1$ (dashed line with squares) and $n = 2$ (dotted line with circles) at the non-reflecting duct outlet $x = L$.

920 Hz for $n = 1$ and $n = 2$ respectively, based on the sound speed downstream of the flame $\bar{c}_2$), the acoustic wave decays with downstream distance and its magnitude is x dependent. The results presented here are at a non-reflecting duct exit a distance $L = 0.5$ m downstream of the combustion zone. Figure 14a shows that for the plane wave $n = 0$, the amplitude of the acoustic wave is independent of frequency. This is consistent with the analytical result in Eq. (42d) which clearly demonstrated that for $n = 0$, the amplitude of the acoustic wave transfer function only depends on temperature ratio and is independent of frequency. Figure 14a shows that for $n > 0$, at low frequencies the pressure amplitude away from the combustion zone is exponentially small because the waves are cut-off. The magnitude of $|\hat{p}/\hat{Q}|$ increases up to a critical frequency. The exact value of the critical frequency can be obtained by investigating the zero of the derivative of Eq. (42b) with respect to ω. It is close to but not at the cut-off frequency based on $\bar{c}_2$. Consequently, it is n dependent, as Fig. 14a shows. As the frequency increases further, the magnitude of $|\hat{p}/\hat{Q}|$ decreases and asymptotes to the plane wave result. This is because as ω tends to infinity, $k_{-1} \approx \omega/\bar{c}_1$ and $-k_{+2} \approx \omega/\bar{c}_2$ and Eq. (42b) simplifies to the plane wave result in Eq. (42d).

Figure 14b illustrates the variation of the entropy wave as a function of frequency for the three circumferential wave numbers. Just as for the acoustic wave, for $n = 0$ the amplitude of the entropy wave transfer function remains constant as the frequency changes. The same conclusion can be made by referring to Eq. (44d) which shows that for the plane waves $|\hat{S}/c_v|/|\hat{Q}/\overline{Q}|$ is independent of frequency depending only on γ and the temperature ratio $\overline{T}_{02}/\overline{T}_{01}$. For $n > 0$, as the frequency tends to zero the magnitude of the entropy wave tends to a non-zero value which from Fig. 14b seems to be independent of n because the results for $n = 1$ and $n = 2$ are similar. This can be confirmed from the analytical form in Eq. (44c). Substituting the low-frequency forms, $k_{-1} = -in/r$ and $k_{+2} = in/r$ into Eq. (44c) shows that the value of $|\hat{S}/c_v|/|\hat{Q}/\overline{Q}|$ is indeed independent of n. In addition it is seen that, similar to the acoustic wave solution, as the frequency becomes high, the results for $n > 0$ asymptote to a value independent of frequency and tend to the solution for plane wave. For a fixed circumferential wave number, there is a minimum and a maximum in the magnitude of entropy wave transfer function. Inspection of Eq. (44c) shows that for $n > 0$ the maximum value of the entropy transfer function occurs at a frequency close to the cut-off frequency based on $\bar{c}_2$ where k_{+2} is nearly zero, while the minimum occurs close to the cut-off frequency based on $\bar{c}_1$ where k_{-1} is small in magnitude.

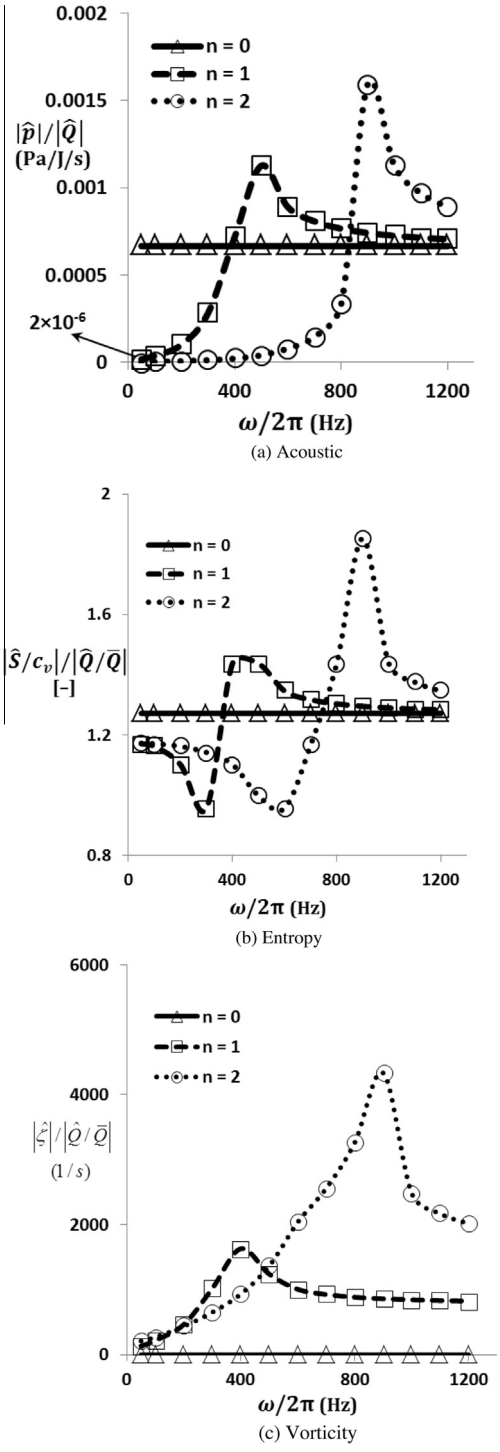

Fig. 14. Magnitude of three waves as a function of frequency obtained for $\overline{M}_{01} = 0.06$ and $\overline{T}_{02}/\overline{T}_{01} = 3$, for circumferential wave numbers $n = 0$ (solid line with triangles), $n = 1$ (dashed line with squares) and $n = 2$ (dotted line with circles) at the non-reflecting duct outlet $x = L$.

The variation of the magnitude of vorticity transfer function with frequency is shown in Fig. 14c. For plane waves there are no vorticity perturbations and hence the value of $|\hat{\zeta}|/|\widehat{Q}/\overline{Q}|$ is zero for $n = 0$. Comparison of Fig. 14c and a shows that for $n > 0$ the vorticity transfer function has a similar dependence on frequency as the pressure perturbation. As noted in Section 7.2.3, this is also clear from a comparison of Eqs. (42b) and (47b). The reason is that for a fixed temperature ratio, the gradient of mean density is constant. Thus, according to Eq. (46c), $\partial p'/\partial \theta = inp'$ determines the strength of vorticity wave giving the magnitude of the vorticity wave the same dependence on frequency as the acoustic pressure at the combustion zone.

9.2.3. Effect of temperature ratio

Effects of the temperature ratio across the combustion zone on the acoustic, entropy and vorticity waves are shown in Fig. 15 for an inlet Mach number of 0.06 and frequency of 200 Hz at a distance $x = L$ downstream of the combustion zone. Since this frequency is below the cut-off frequencies for circumferential modes $n = 1$ and 2, the pressure transfer function is exponentially small, e.g. for $n = 2$ and $\overline{T}_{02}/\overline{T}_{01} = 1.5$ we have $|\hat{p}|/|\widehat{Q}| = 2.0 \times 10^{-5}$ Pa J^{-1}s, and for $\overline{T}_{02}/\overline{T}_{01} = 5$ we obtain $|\hat{p}|/|\widehat{Q}| = 4.0 \times 10^{-6}$ Pa J^{-1}s. Figure 15a shows that as $\overline{T}_{02}/\overline{T}_{01} \to 1$, the magnitude of $|\hat{p}/\widehat{Q}|$ tends to a non-zero number. This can be readily obtained by substituting $T_R = 1$ into Eq. (42b). As noted in Section 7.2.1, heat release fluctuations generate acoustic waves even when there is no mean heat input. As the temperature ratio across the combustion zones increases, the magnitude of $|\hat{p}/\widehat{Q}|$ decreases. This is consistent with the low Mach number analytical solution in Eq. (42d) where we found the magnitude to be proportional to $(1 + T_R^{1/2})^{-1}$ for $n = 0$. In addition, it is seen that for a fixed temperature ratio, as n increases the magnitude of the acoustic wave decreases and $n = 0$ yields the highest magnitude. This is because 200 Hz is below the cut-off frequency for $n \neq 0$ and the acoustic waves decay exponentially with distance along the duct with a rate that increases with n.

Figure 15b shows the variation of $|\widehat{S}/c_v|/|\widehat{Q}/\overline{Q}|$ as a function of temperature ratio. It tends to zero as the temperature ratio $\overline{T}_{02}/\overline{T}_{01} \to 1$. It is seen that for a fixed n as the temperature ratio increases the magnitude of this entropy transfer function increases but not as rapidly as linearly. For high temperature ratios, it is constant and does not change with $\overline{T}_{02}/\overline{T}_{01}$. This is all consistent with the low Mach number analytical form in Eq. (44c). The strength of the entropy wave itself described by $|\widehat{S}/\overline{Q}|$ actually decreases as the temperature ratio decreases. This can also been seen from Eq. (44c). Interesting to note is

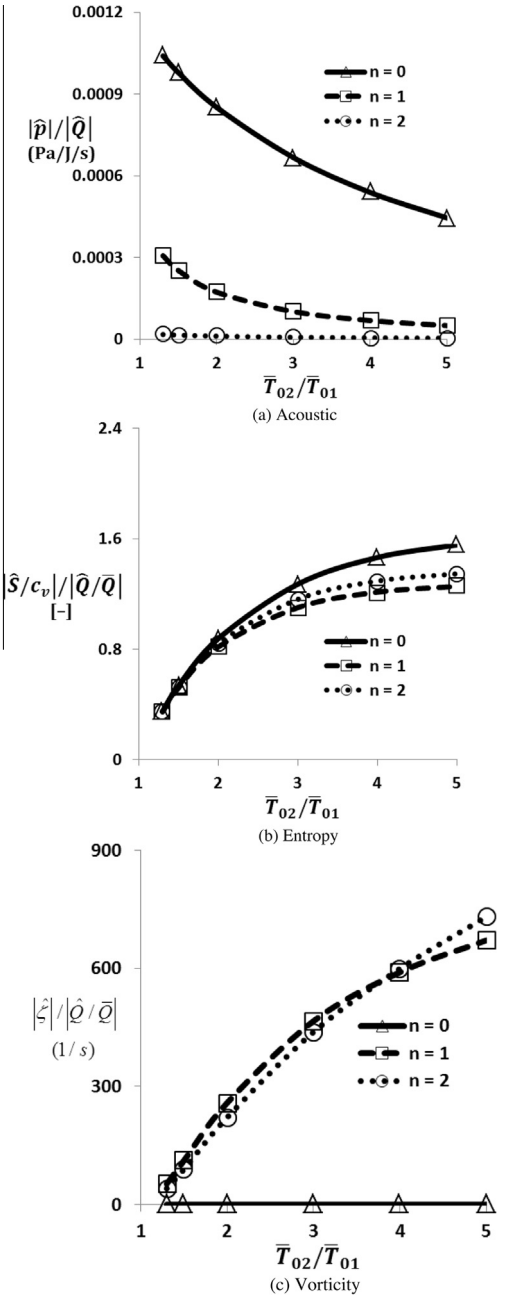

Fig. 15. Magnitude of three waves as a function of $\overline{T}_{02}/\overline{T}_{01}$ obtained for $\overline{M}_{01} = 0.06$ and $f =$ 200 Hz, for circumferential wave numbers $n = 0$ (solid line with triangles), $n = 1$ (dashed line with squares) and $n = 2$ (dotted line with circles) at the non-reflecting duct outlet $x = L$.

that as $\overline{T}_{02}/\overline{T}_{01} \to 1$, the magnitude of the entropy wave $|\widehat{S}/\overline{Q}|$ tends to a finite non-zero number (although $|\widehat{S}/c_v|/|\widehat{Q}/\overline{Q}| \to 0$). As noted in Section 7.2.2, entropy waves can be generated by heat

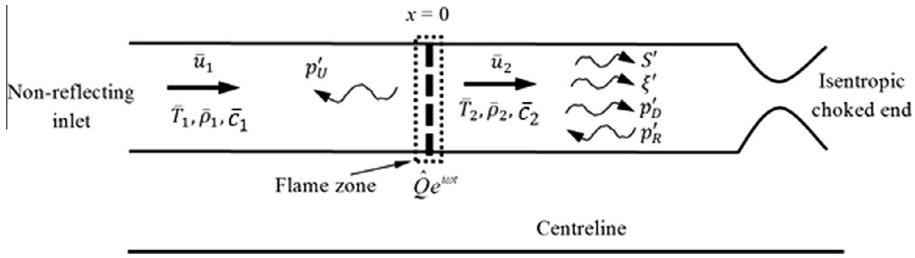

Fig. 16. One-dimensional disturbances in simple combustor with a choked exit nozzle and a mean flow and mean rate of heat release.

release fluctuations even in the case of zero mean heat release rate. In contrast to Fig. 15a, in which the magnitude of the acoustic pressure wave is highly n dependent, Fig. 15b shows that changes in n only have a weak effect on the magnitude of entropy wave. This is particularly true for low temperature ratios, where as shown in Eq. (44c), it is independent of n.

Figure 15c for the vorticity wave confirms again that for plane waves the magnitude of the vorticity wave is zero. It is further seen that as $\overline{T}_{02}/\overline{T}_{01} \to 1, |\hat{\zeta}/(\widehat{Q}/\overline{Q})|$ tends to zero. As the temperature ratio increases, $|\hat{\zeta}|/|\widehat{Q}/\overline{Q}|$ increases but not as fast as linearly. For small frequencies and $n \neq 0$, $k_{-1} = -in/r$ and $k_{+2} = in/r$. Substituting into Eq. (48) shows that as temperature ratio increases, $|\hat{\zeta}|/|\widehat{Q}/\overline{Q}|$ increases as $\omega(1 - T_R^{-1})$, i.e. independent of n. This is consistent with the results in Fig. 15c which show that the difference between the magnitude of vorticity wave for the two circumferential wave numbers $n = 1$ and $n = 2$ is small.

9.3. Results for choked outlet nozzle

In this section the interaction of acoustic, entropy and vorticity waves at an exit nozzle is studied. The configuration considered in this section is shown in Fig. 16. The outlet is choked so that the non-dimensional mass flow rate is constant there.

Upstream of the zone of heat input there is an upstream propagating acoustic wave (p'_U). Downstream of the combustion zone, acoustic (p'_D), entropy (S') and vorticity $(\vec{\xi}')$ waves produced by the flame, travel downstream toward the nozzle contraction, where they are partially reflected to give an upstream propagating acoustic wave (p'_R). This interacts with the flame to produce a transmitted wave altering (p'_U) upstream of the flame in $x < 0$. It also alters the downstream propagating acoustic, entropic and vortical waves. LOTAN calculates this complex wave pattern. The mean flow is uniform upstream and downstream of the zone of heat release and so linear perturbations in those regions will be the superposition of disturbances of the form shown in Section 7.1. Equations of conservation of mass, momentum and energy are used across the flame zone to relate the waves on either side as discussed in Section 7.2 and the choked end boundary condition in Eq. (50) is applied in the straight-walled duct just upstream of the nozzle contraction.

As well as determining the linear waves generated, we also want to separate out the individual contributions from the direct noise (acoustic waves generated directly by unsteady combustion) and indirect noise (acoustic waves generated by the interaction of entropy and vorticity waves with the exit nozzle). To calculate the direct sound, we still calculate the entropy and vorticity waves generated at the flame but ignore their contribution when applying the downstream boundary condition. This means that the reflected wave depends only on the incident sound wave and the acoustic pressure fluctuations are uncoupled from entropy and vorticity disturbances. The direct sound field in $x > 0$ is then obtained by adding the downstream and upstream propagating acoustic waves. The indirect noise due to the entropy and vorticity waves incident on the choked nozzle can be determined by subtracting the direct noise from the full sound field calculated with all the incident waves contributing to the acoustic wave reflected from the nozzle. The magnitude of the direct and indirect noise transfer functions have been investigated numerically using LOTAN for three circumferential mode numbers, a wide range of frequencies, stagnation temperature ratios and inlet Mach numbers.

In order to study the effect of a choked exit on the magnitude of the acoustic waves produced by the flame, the transfer function $|\hat{p}/\widehat{Q}|$ is shown as a function of temperature ratio for the plane wave $n = 0$ in Fig. 17. It is seen that compared to the non-reflecting case, the choked exit approximately doubles the magnitude of the pressure perturbation at the exit. This is not surprising. In a low Mach number mean flow, the choked end boundary condition in Eq. (50) approximates to a hard end boundary condition $\hat{u} = 0$ for an incident plane sound wave. This leads to a reflected wave of equal amplitude, and hence to a pressure

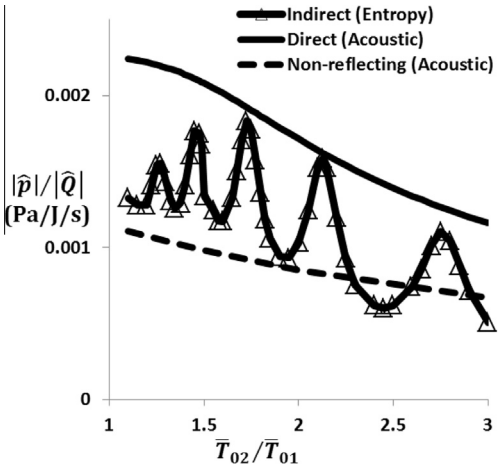

Fig. 17. Magnitude of the indirect entropy noise (solid line with triangle), direct noise (solid line) and acoustic noise for non-reflecting outlet (dashed line) as function of temperature ratio obtained for plane wave ($n = 0$), $\overline{M}_{01} = 0.06$ and $f = 550$Hz just upstream of the nozzle.

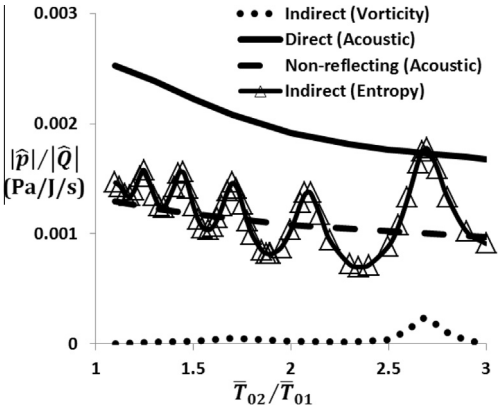

Fig. 18. Magnitude of indirect vorticity noise (dotted line), indirect entropy noise (solid line with triangle), direct noise (solid line) and acoustic noise for non-reflecting outlet (dashed line) as function of temperature ratio obtained for circumferential mode ($n = 1$), $\overline{M}_{01} = 0.06$ and $f = 550$Hz just upstream of the nozzle.

doubling just upstream of the exit nozzle. In addition, the choked end converts an incoming convected entropy disturbance into indirect noise.

It is seen that although the indirect noise generated is similar in magnitude to the incident acoustic wave in the case with a non-reflecting boundary, it is usually smaller than the exit pressure in the multiple reflected field that makes up direct noise with a choked exit. Nevertheless, it is large enough to contribute to the high amount of total noise. The indirect noise has more complicated dependency on the temperature ratio than the direct acoustic wave which decreases gradually with the temperature ratio. In contrast, the indirect sound has multiple peaks and troughs. This is due to resonances caused by multiple reflections of waves between the choked nozzle and the upstream geometry, an effect that is clearer in the variation with frequency plotted in Fig. 19. In the simple geometry we are considering with a non-reflecting inlet, the upstream reflection occurs at the flame zone and is due to the change in the mean flow conditions across the combustion zone. Hence as the temperature ratio tends to 1, the reflection from the combustion zone gets weaker and the variation in the amplitude of indirect noise is reduced.

Figure 18 shows results for circumferential mode number $n = 1$. Just as in Fig. 17, the transfer function $|\hat{p}/\hat{Q}|$ at the duct exit is shown for a frequency of 550 Hz (which is above the cut-off frequency) and varying temperature ratios. Again it is seen that the choked end increases the magnitude of the direct noise, as it did for the plane wave in Fig. 17. At low temperature ratios the amount of indirect noise due to the vorticity perturbation is found to be two orders of magnitude smaller than the direct wave. Although the magnitude of the direct noise decreases at higher temperature ratios, the indirect noise due to the vorticity wave is still one order of magnitude smaller. Thus, it is concluded that the vorticity wave has negligible contribution to the noise generation at the low mean flow Mach numbers typical of gas turbine combustors. This is in agreement with the simple analytical solution presented in Eq. (39b). Just as for the plane wave, the indirect noise due to the entropy has multiple peaks and troughs due to the resonances. At low temperature ratios the direct noise is nearly twice the indirect entropy noise, whereas at a particular higher temperature ratio a resonance can make the magnitude of the entropy noise comparable to that of the direct noise.

The transfer function $|\hat{p}/\hat{Q}|$ just upstream of the nozzle at the duct exit is shown as a function of frequency in Fig. 19 for a choked exit nozzle, three circumferential mode numbers and an inlet Mach number of 0.06 and stagnation temperature ratio of 3. Resonances are observed in both the direct and indirect sound, but with different frequency intervals between the peaks and troughs. For the plane wave in Fig. 19a we expect resonances in the direct acoustic wave to be related to the sum of the time taken for acoustic waves to travel a distance L from combustion zone to nozzle $(L/(\bar{c}_2 + \bar{u}_2))$ and back $(L/(\bar{c}_2 - \bar{u}_2))$. This adds up to $2L\bar{c}_2/\left(\bar{c}_2^2 - \bar{u}_2^2\right)$ which is approximately $2L/\bar{c}_2$ in this low Mach number mean flow. So we expect the gap between resonant frequencies to be about $\bar{c}_2/(2L)$ Hz (approximately 900 Hz for the conditions in Fig. 19). For the

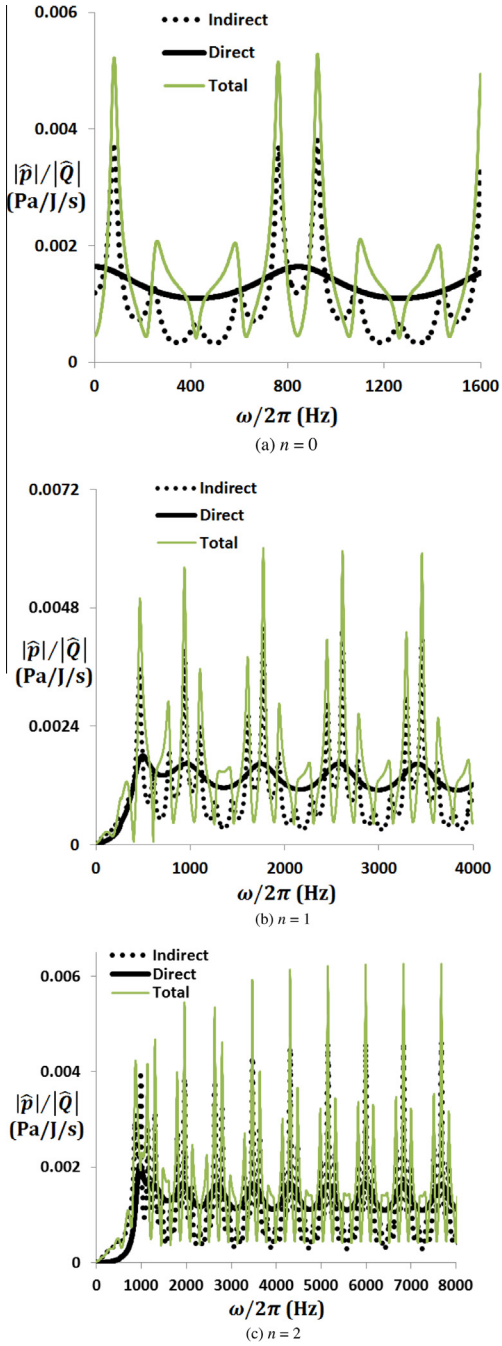

Fig. 19. Variation of indirect noise (dotted line), direct noise (solid line) and total noise (green line) as function of frequency obtained for $\overline{M}_{01} = 0.06$ and $\overline{T}_{02}/\overline{T}_{01} = 3$ just upstream of the nozzle for circumferential mode (a) $n = 0$, (b) $n = 1$ and (c) $n = 2$.

indirect entropy noise, the relevant time is based on convection from the combustion zone to the nozzle ($L/\overline{u}_2$) and acoustic propagation back upstream ($L/(\overline{c}_2 - \overline{u}_2)$). For a low Mach number mean flow this cycle time is approximately ($L/\overline{u}_2$) leading to a very much smaller frequency interval $\overline{u}_2/L$ Hz (approximately 180 Hz for the conditions in Fig. 19). When acoustic and entropic resonances coincide, the indirect noise is seen to be much higher than the direct noise. It contributes significantly to the overall pressure perturbation throughout this frequency range.

For the first circumferential mode ($n = 1$), Fig. 19b shows that at frequencies below cut-off (~460 Hz), the acoustic wave is exponentially small and thus the magnitude of the indirect noise is higher than direct noise but even this is small compared with the comparable transfer function for the plane wave for low frequencies (< 200 Hz). For frequencies above cut-off, the acoustic waves propagate and the magnitude of the direct noise increases and becomes comparable to the indirect noise. Again similar to the plane wave, resonances are observed in both the direct and indirect noise with the frequency gap between resonances being much smaller for the indirect than for the direct noise. When acoustic and entropic resonances coincide particularly high contributions occur from the indirect noise. These combined resonances occur at frequencies of 461, 935, 1770, 2601 and 3450. Only the lowest is likely to be of practical interest because the entropy waves will be attenuated by diffusion at the higher frequencies.

A similar pattern is observed for the higher circumferential mode ($n = 2$) shown in Fig. 19c where the cut-off frequency is now about 920 Hz. At frequencies below cut-off, the magnitude of the indirect noise is predicted to be higher than the direct noise. It is seen that the maximum value of the direct noise occurs at the frequency close to the cut-off frequency of 920 Hz. This is similar to the results presented in Fig. 14a for the non-reflecting end condition.

The results presented in this section have shown that the main indirect source is due to entropy: the vorticity wave makes only a small contribution to the overall sound pressure in the low Mach number flows in a gas turbine. The indirect sound due to entropy fluctuations convecting through a choked nozzle can be comparable to the direct sound due to the acoustic waves directly generated by the unsteady combustion. Both direct and indirect sound exhibit resonances, and a prediction of their relative importance requires a detailed calculation of the linear waves in the combustor and depends the geometry, boundary conditions and on the mean flow. The indirect sound pressure can be particularly intense at frequencies that are harmonics of both the entropic and the acoustic resonances.

10. Conclusions, open questions and future research

This paper has discussed some of the progress made in understanding combustion noise and examined the challenges to be faced, focusing on the contribution from the different combustion noise sources in an aeroengine combustor.

Early studies investigated the noise from flames in unbounded space. For such open flames, there is analytical solution for the pressure fluctuations generated by specified fluctuations in heat release rate: the pressure perturbation depends on the rate of change of the rate of combustion at an earlier time which takes into account the time taken for sound to travel from the combustion source to the listener and decays inversely with distance from the source. When the combustion zone is compact (i.e. its linear dimension is small in comparison with the speed of sound divided by the frequency) and the listener is far away compared with the wavelength, this time delay is effectively the same across the combustion zone. The mean square pressure generated by open flames then depends on the product of mean square value of the rate of change of heat release multiplied by the correlation volume of this stochastic source, integrated over the combustion zone (see Eq. (5)). This illustrates how the investigation of combustion noise decouples into two distinct elements: one is the determination of the statistics of the unsteady heat release in a turbulent flame and the other is the generation of noise by these heat release fluctuations. The latter is an acoustic problem, there is an analytical solution in free space and even with the complicated geometry of a gas turbine semi-analytical techniques based on linear waves can be used. The evaluation of the unsteady heat release and how this quantity scales with underlying turbulence parameters is a far more difficult problem, right at the heart of turbulent combustion modelling, and has many challenges and uncertainties. Therefore, most of the early studies used basic physical scaling, or semi-empirical correlations of these unknown parameters, in order to derive combustion noise models [31,32,56].

For an aeroengine real combustor, combustion takes place in confined geometry and sound generation occurs not only directly due to fluctuations in the rate of heat release in the combustion zone but also indirectly as hot-spots convect through the nozzle. In addition, the directly generated acoustic waves are multiply reflected by the boundaries of the combustor. High-fidelity methods for compressible reacting flows, e.g. Large Eddy Simulation (LES) have been used extensively in the field of turbulent combustion to predict the mean flow fields [34,120,121] in turbulent flames. They have been also utilized in the investigations of combustion instabilities and combustion noise in swirled combustors [122–124]. The LES methodology can be applied in either fully compressible or low Mach number tools for reacting flows coupled to computational aeroacoustics (CAA) approaches for the propagation of acoustic waves [52,125]. Direct Numerical Simulation (DNS) of simple flames has been used to investigate the correlation volume of fluctuations in the rate of heat release, a vital parameter when predicting the combustion noise [31].

Hybrid methods or two-step methods have been developed over the last decade. These approaches take advantage of the length scale separation between a subsonic flow field and the acoustic field which is generated by this flow [126–129]. In low Mach number flows, the fluid dynamic and acoustic length scales are separated by more than an order of magnitude [125]. In a first step, the turbulent flow is computed by a highly resolved solution of the conservation equations. This information is used to determine the source terms of some set of acoustic equations which are then solved to give the sound field. In this method it is necessary to determine the dominant combustion sources, which can be efficiently computed using standard methods such as LES to analyse flame physics [52,130,131], and then use a CAA technique to predict the acoustic field generated by these sources.

The acoustics of a gas turbine combustor requires consideration of the whole geometry through which acoustic waves propagate which is from compressor exit to turbine entry. The analysis of linear waves is made easier when the cross-stream dimension of the combustor is small compared with the acoustic wavelength. Then acoustic modes with variations across the cross-section are 'cut-off', decaying with axial position rather than propagating, and variations of the acoustic waves across the cross-section can be neglected. This leads to plane waves in a cylindrical combustor and axial and circumferential waves in an annular combustor. The frequencies of interest for combustion noise in aeroengines are sufficiently low that this is often a good approximation. Then the linear wave equations can be solved semi-analytically by a network approach. This enables physical insight into important mechanisms. Even without full knowledge of turbulent combustion noise sources some general conclusions can be made about the combustion noise in gas turbine combustors. This is because the direct combustion noise and the entropy fluctuations, which are the cause of the indirect noise, are both related to the unsteady rate of combustion. By looking at the transfer functions between acoustic and entropic waves and the rate of heat release we can investigate the relative importance of the direct and indirect sound at different mean flow conditions for different frequencies and mode numbers.

We looked first at the generation of acoustic, entropic and vorticity perturbations in a model

combustor. We found that the strength of the generated entropy wave was such that its first reflection at a choked nozzle always made a bigger contribution to the reflected acoustic wave than the incident sound wave (see Fig. 9). Multiple reflections can change this simple conclusion with the acoustic and entropic disturbances having resonances due to multiple reflections in the combustor geometry. Each can be enhanced to be the most important at its resonant frequency. In particular, the indirect entropy sound pressure can be particularly intense at frequencies that are harmonics of both the entropic and the acoustic resonances.

For circumferential mode numbers $n \geqslant 1$, vorticity fluctuations are generated due to the baroclinic vorticity production mechanism involving the product of the gradient of pressure wave in the circumferential direction and the gradient of mean density across the flame. However, we have shown that this vorticity wave does not generate significant noise in the low mean flow Mach numbers in aeroengine combustors.

Although the simple calculations described here and other recent efforts explain the basic mechanism of generation and propagation of acoustic, entropy and vorticity waves, the prediction of the contribution of indirect to direct combustion noise that would occur in real aeroengine combustors still poses important scientific challenges. There are a number of issues and questions that need further investigation. For example, to predict absolute levels rather than comparison between relative levels of direct and indirect noise better models of the statistics of the unsteady combustion are needed. Other open questions include: How do better 2-D acoustic computations of choked exit nozzle, affect the computed amount of indirect noise generated? What is the dominant dispersion mechanism of entropy waves in combusting flows and how does this affect the amount of indirect noise generated?

The exit nozzle is the bridge between entropy disturbances and the indirect noise they radiate [7]. The existing theories describing the nozzle dynamics make a number of simplifying assumptions, such as one-dimensionality and compactness (e.g. [12,30,78,89,98]). Recent experimental studies, however, have showed that some of these assumptions, particularly on one-dimensionality, are questionable [106]. To develop a two-dimensional model for the response of choked nozzle to entropic disturbances, further numerical simulations need to be conducted to determine the acoustic waves reflected and transmitted when entropy fluctuations convect through an extensive nozzle.

Another important issue in the problem of combustion noise is the dispersion of entropy waves. Turbulent mixing and diffusion can contribute to the reduction in the amplitude of the entropy disturbances as they convect from the combustion zone to the nozzle [109]. In addition variations of the mean flow velocity across the combustor will tend to spread out the entropy fluctuations due to differences in their convection time. The decay of entropy disturbances and its spatial distribution should be further explored.

In real aeroengine combustors, the impact and importance of entropy noise is a controversial issue as pointed out by Strahle [41], mainly due to the lack of comprehensive experimental data. One of the main challenges in experimental investigation of entropy noise is the separation of direct and indirect combustion noise. For example, characterizing the entropy waves entering a turbine stage or a nozzle requires measurement of temperature fluctuations spatially and temporally in a high-speed reacting flow. Acoustic waves generated by this interaction are also difficult to measure and require great care. Ideally, theory, experiments and numerical methods need to be used together to understand noise sources in real engines. To achieve this goal, two difficulties need to be overcome: (1) Acoustic boundary conditions of the combustion chamber must be known and preferably controllable. (2) The entropy fluctuations need to be measured. On the experimental side separation of different effects can be obtained by controlling and independently introducing acoustic, entropic or vortical waves. Experiment [94] and numerical investigations [78] have shown that indirect combustion noise can be a significant source of noise in an experimental combustor configuration. However, the relative contribution of the two acoustic source mechanisms in a realistic aero-engine combustor has not been fully demonstrated. In fact, recent measurements suggest that this is dependent on geometry, operating conditions, and frequency range [8]. The extreme operating conditions add complexity and make this a challenging experiment under real engine conditions.

In this paper we only discussed the indirect noise generated by the interaction of the entropic disturbances with the choked nozzle at exit to the combustion chamber. However, in an aeroengine, any entropy fluctuations that persist into the turbine will similarly generate acoustic waves as they interact with each stage of the turbine. This mechanism modifies the overall level of combustion noise radiated in far field and must therefore be better understood. There are turbomachinery approaches based on actuator-disk theory that enable such interactions to be evaluated, but currently most low-order models ignore the dispersion of entropy waves. The entropy and acoustic wave interaction needs to be investigated experimentally on a realistic turbine and the results of CFD turbomachinery solvers and low-order analytical codes compared to the experimental results to investigate the dispersion of the entropy waves as they pass through the turbine blade rows.

Currently lack of knowledge about the entropy wave dispersion adversely affects the ability of such models to predict the radiated combustion noise from aeroengines.

Acknowledgements

The authors acknowledge financial support through European Commission in the Seventh Framework Programme FP7 under Grant Agreement No. ACP2-GA-2012–312444 in RECORD (Research on Core Noise Reduction) project. We would like to thank the SAFRAN Snecma company for providing us with Fig. 2 showing the contribution of noise sources on a turbojet engine.

References

[1] ICAO Circular 313: Outlook for Air Transport to the Year 2025 (2007).
[2] M.J.T. Smith*Aircraft Noise*, vol. 3, Cambridge University Press, UK, 2004.
[3] W.C. Strahle, *J. Sound Vibr.* 23 (1972) 113–125.
[4] Y. Liu, A.P. Dowling, N. Swaminathan, R. Morvant, M.A. Macquisten, L.F. Caracciolo, *J. Propul. Power* 30 (2013) 114–122.
[5] A.P. Dowling, S.R. Stow, *J. Propul. Power* 19 (2003) 751–764.
[6] T. Lieuwen, V. Yang, Combustion Instabilities in Gas Turbine Engines: Operational Experience, Fundamental Mechanisms, and Modeling, Progress in Astronautics and Aeronautics, vol. 210, AIAA, Washington, 2005.
[7] A.P. Dowling, S.R. Stow, Acoustic Analysis of gas turbine combustors, in: Combustion Instabilities in Gas Turbine Engines: Operational Experience, Fundamental Mechanisms, and Modeling. Progress in Astronautics and Aeronautics, AIAA, Reston, Virginia, USA, pp. 369–414. ISBN 156347669X, 2005.
[8] C.K.W. Tam, N.N. Pastouchenko, J. Mendoza, D. Brown, Combustion Noise of Auxiliary Power Units, AIAA Paper 2829 (2005) no. 11.
[9] C.K.W. Tam, S.A. Parrish, J. Xu, B. Schuster, *J. Sound Vibr.* 332 (2013) 4004–4020.
[10] S. Candel, D. Durox, S. Ducruix, A.L. Birbaud, N. Noiray, T. Schuller, *Int. J. Aeroacoustics* 8 (2009) 1–56.
[11] W.C. Strahle, *Prog. Energy Combust. Sci.* 4 (1978) 157–176.
[12] F.E. Marble, S. Candel, *J. Sound Vibr.* 55 (1977) 225–243.
[13] S. Bragg, *J. Inst. Fuel* 36 (1963) 12–16.
[14] A. Thomas, G.T. Williams, *Proc. Roy. Soc. Lond. Ser. A* 294 (1966) 449–466.
[15] A.P. Dowling, J.E. Ffowcs Williams, *Sound and Sources of Sound*, Ellis Horwood Limited, Chichester, UK, 1983.
[16] C.L. Morfey, *J. Sound Vibr.* 31 (1973) 391–397.
[17] J.E. Ffowcs Williams, M.S. Howe, *J. Fluid Mech.* 70 (1975) 605–622.
[18] M.S. Howe, *J. Fluid Mech.* 659 (2010) 267–288.
[19] B.T. Chu, L.S.G. Kov'asznay, *J. Fluid Mech.* 3 (1958) 494–514.
[20] C. Richter, Ł. Panek, V. Krause, F. Thiele, *Investigations regarding the simulation of wall noise interaction and noise propagation in swirled combustion chamber flows, in: Combustion Noise*, Springer, Berlin, Heidelberg, 2009, pp. 217–238.
[21] J.W.S. Rayleigh, *Nature* 18 (1878) 319–321.
[22] J.W.S. Rayleigh, *The Theory of Sound*, 2nd ed., Dover Publications, New York, 1945.
[23] F. Culick, V. Yang, *Progress in astronautics and aeronautics: liquid rocket engine combustion instability*, *AIAA* 169 (1995) 3–37, Ch. 1: Overview of combustion instabilities in liquid-propellant rocket engines.
[24] Z. Yao, Y. Gao, M. Zhu, A.P. Dowling, K.N.C. Bray, *J. Propul. Power* 28 (2012) 1015–1025.
[25] W. Polifke, C.O. Paschereit, K. Döbbeling, *Int. J. Acoust. Vibr.* 6 (2001) 135–146.
[26] C.H. Goh, A.S. Morgans, *Combust. Sci. Technol.* 185 (2013) 249–268.
[27] A.S. Morgans, A.M. Annaswamy, *Combust. Sci. Technol.* 180 (2008) 1549–1571.
[28] J. Eckstein, F. Freitag, C. Hirsch, T. Sattelmayer, Experimental study on the role of entropy waves in low-frequency oscillations for a diffusion burner, in: ASME Turbo Expo 2004: Power for Land, Sea, and Air, American Society of Mechanical Engineers, pp. 743–751.
[29] J.H. Miles, *J. Propul. Power* 25 (2009) 218–227.
[30] C.H. Goh, A.S. Morgans, *J. Sound Vibr.* 330 (2011) 5184–5198.
[31] N. Swaminathan, G. Xu, A.P. Dowling, R. Balachandran, *J. Fluid Mech.* 681 (2011) 80–115.
[32] H.A. Hassan, *J. Fluid Mech.* 66 (1974) 445–453.
[33] S. Kotake, K. Takamoto, *J. Sound Vibr.* 112 (1987) 345–354.
[34] M. Ihme, H. Pitsch, *Int. J. Aeroacoust.* 11 (2012) 25–78.
[35] R.B. Price, I.R. Hurle, T.M. Sugden, *Symp. (Int.) Combust.* 12 (1968) 1093–1102.
[36] I. Hurle, R. Price, T. Sudgen, A. Thomas, *Proc. Roy. Soc. Lond. A* 303 (1968) 409–427.
[37] T. Smith, J. Kilham, *J. Acoust. Soc. Am.* 35 (1963) 715–724.
[38] B.N. Shivashankara, W.C. Strahle, J.C. Handley, *AIAA J.* 13 (1975) 623–627.
[39] D.G. Crighton, A.P. Dowling, J.E. Ffowcs Williams, M. Heckl, F.G. Leppington, *Modern Methods in Analytical Acoustics*, Springer-Verlag, 1992, Chapter13.
[40] M.J. Lighthill, *Proc. Roy. Soc. Lond. A* 211 (1952) 564–587.
[41] W.C. Strahle, *J. Fluid Mech.* 49 (1971) 399–414.
[42] C. Hirsch, J. Wasle, A. Winkler, T. Sattelmayer, *Proc. Combust. Inst.* 31 (2007) 1435–1441.
[43] L. Kabiraj, H. Nawroth, A. Saurabh, C.O. Paschereit, Experimental Study of Noise Generation by a Turbulent Premixed Flame, 19th AIAA/CEAS Aeroacoustics Conference, 2013.
[44] J.H. Kilham, N. Kirmani, *Proc. Combust. Inst.* 17 (1979) 327–336.
[45] R. Rajaram, T. Lieuwen, *Combust. Sci. Technol.* 175 (2003) 2269–2298.
[46] R. Rajaram, T. Lieuwen, *J. Fluid Mech.* 637 (2009) 357–385.

[47] W.C. Strahle, B.N. Shivashankara, *Proc. Combust. Inst.* 15 (1975) 1379–1385.
[48] T. Lieuwen, S. Mohan, R. Rajaram, *Combust. Flame* 144 (2006) 360–369.
[49] N. Ohiwa, K. Tanaka, S. Yamaguchi, *Combust. Sci. Technol.* 90 (1993) 61–78.
[50] S.A. Klein, J.B.W. Kok, *Combust. Sci. Technol.* 149 (1999) 267–295.
[51] K.K. Singh, S.H. Frankel, J.P. Gore, *AIAA J.* 42 (2004) 931–936.
[52] F. Flemming, A. Sadiki, J. Janicka, *Proc. Combust. Inst.* 31 (2007) 3189–3196.
[53] M. Ihme, H. Pitsch, D. Bodony, *Proc. Combust. Inst.* 32 (2009) 1545–1553.
[54] K.K. Singh, C. Zhang, J.P. Gore, L. Mongeau, S.H. Frankel, *Proc. Combust. Inst.* 30 (2005) 1707–1715.
[55] P. Duchaine, L. Zimmer, T. Schuller, *Proc. Combust. Inst.* 32 (2009) 1027–1034.
[56] N. Swaminathan, R. Balachandran, G. Xua, A.P. Dowling, *Proc. Combust. Inst.* 33 (2011) 1533–1541.
[57] Y. Liu, A.P. Dowling, T.D. Dunstan, N. Swaminathan, Modeling of combustion noise spectrum from turbulent premixed flames, in: Proc. Acoustics 2012, Nantes, France, 2012.
[58] K.K. Singh, S.H. Frankel, J.P. Gore, *AIAA J.* 41 (2003) 319–321.
[59] M.J. Lighthill, *Proc. Roy. Soc. Lond. A* 222 (1954) 1–32.
[60] J. Truffaut, G. Searby, L. Boyer, *Combust. Theory Model* 2 (1998) 423–428.
[61] T.C. Lieuwen, *Unsteady Combustor Physics*, Cambridge University Press, UK, 2012.
[62] C. Bailly, C. Bogey, S. Candel, *Int. J. Aeroacoust.* 9 (2010) 461–490.
[63] G.M. Lilley, The Generation and Radiation of Supersonic Jet Noise. Vol. IV—Theory of Turbulence Generated Jet Noise, Noise Radiation from Upstream Sources, and Combustion Noise. Part II: Generation of Sound in a Mixing Region. Part II: Generation of Sound in a Mixing Region, Air Force Aero Propulsion Laboratory AFAPL-TR-72-53, (4), 1972.
[64] S. Kotake, *J. Sound Vibr.* 42 (1975) 399–410.
[65] A.J. Kempton, *J. Fluid Mech.* 78 (1976) 1–31.
[66] Y.L. Sinai, *J. Fluid Mech.* 99 (1980) 383–397.
[67] A. Powell, *J. Acoust. Soc. Am.* 36 (2005) 177–195.
[68] A.P. Dowling, Mean Temperature and Flow Effects on Combustion Noise, AIAA paper 1 (1976).
[69] W.C. Strahle, 14th Symp. (Int.) Combust. (1973) 527–535.
[70] P. Palies, D. Durox, T. Schuller, S. Candel, *J. Fluid Mech.* 672 (2013) 545–569.
[71] J.H. Horlock*Actuator Disk Theory – Discontinuities in Thermo-Fluid Dynamics*, Vol. 256, McGraw-Hill, International Book Co., New York, 1978.
[72] S. Kaji, T. Okazaki, *J. Sound Vibr.* 11 (1970) 339–353.
[73] W. Koch, *J. Sound Vibr.* 18 (1971) 111–128.
[74] C.L. Morfey, *J. Sound Vibr.* 28 (1973) 587–617.
[75] M.S. Howe, *J. Fluid Mech.* 71 (1975) 625–673.
[76] N.A. Cumpsty, F.E. Marble, *J. Sound Vibr.* 54 (1977) 297–309.
[77] N.A. Cumpsty, *J. Sound Vibr.* 66 (1979) 527–544.
[78] M. Leyko, F. Nicoud, T. Poinsot, AIAA J., 0001-1452, 47(11) (2009) 2709–2716.
[79] S.R. Stow, A.P. Dowling, T.P. Hynes, *J. Fluid Mech.* 467 (2002) 215–239.
[80] M.S. Bohn, *J. Sound Vibr.* 52 (1977) 283–297.
[81] A.W. Bloy, *J. Fluid Mech.* 93 (1979) 465–475.
[82] M. Huet, A. Giauque, *J. Fluid Mech.* 733 (2013) 268–301.
[83] A.P. Dowling, S. Hubbard, *Proc. Inst. Mech. Eng. Part A: J. Power Energy* 214 (2000) 317–332.
[84] T. Sattelmayer, *J. Eng. Gas Turbines Power* 125 (2003) 11–19.
[85] M.J. Brear, F. Nicoud, M. Talei, A. Giauque, E.R. Hawkes, *J. Fluid Mech.* 1 (2012) 1–21.
[86] S. Hochgreb, D. Dennis, I. Ayranci, W. Bainbridge, S. Cant, Forced and self-excited instabilities from lean premixed, liquid-fuelled aeroengine injectors at high pressures and temperatures, in: Proc. ASME Turbo Expo, Paper GT2013-95311, 2013.
[87] E. Motheau, Y. Mery, F. Nicoud, T. Poinsot, *J. Eng. Gas Turbines Power* 135 (2013) 092602.
[88] N.A. Cumpsty, F.E. Marble, *Proc. Roy. Soc. Lond. A* 357 (1977) 323–344.
[89] W.H. Moase, M.J. Brear, C. Manzie, *J. Fluid Mech.* 585 (2007) 281–304.
[90] A. Giauque, M. Huet, F. Clero, *J. Eng. Gas Turbines Power* 134 (2012) 111202.
[91] I. Duran, S. Moreau, *J. Fluid Mech.* 723 (2013) 190–231.
[92] M. Muthukrishnan, W.C. Strahle, D. Neale, *AIAA J.* 16 (1978) 320–327.
[93] E.E. Zukoski, J.M. Auerbach, *J. Eng. Power* 98 (1976) 60–63.
[94] F. Bake, U. Michel, I. Röhle et al., Indirect combustion noise generation in gas turbines, AIAA Paper 2005–2830 (2005).
[95] F. Bake, C. Richter, B. Mühlbauer, et al., *J. Sound Vibr.* 326 (2009) 574–598.
[96] F. Bake, N. Kings, A. Fischer, I. Röhle, *Int. J. Aeroacoust.* 8 (2009) 125–142.
[97] N. Kings, L. Enghardt, F. Bake, Indirect combustion noise: experimental investigation of the vortex sound generation in a choked convergent–divergent nozzle, in: Proc. Acoustics 2012, Nantes, France, 2012.
[98] M. Leyko, F. Nicoud, S. Moreau, T. Poinsot, *Comptes Rendus Mécanique* 337 (2009) 415–425.
[99] M. Leyko, S. Moreau, F. Nicoud, T. Poinsot, *J. Sound Vibr.* 330 (2011) 3944–3958.
[100] B. Mühlbauer, B. Noll, M. Aigner, *Acta Acustica united with Acustica* 95 (2009) 470–478.
[101] Richter, F. Thiele, *Acta Acustica united with Acustica* 95 (2009) 479–492.
[102] I. Durán, S. Moreau, T. Poinsot, *AIAA J.* 51 (2013) 42–52.
[103] M. Leyko, S. Moreau, F. Nicoud, T. Poinsot, Waves transmission and generation in turbine stages in a combustion–noise framework, in: 16th AIAA/CEAS Aeroacoustics Conference, AIAA Paper, 2010.
[104] I. Duran, M. Leyko, S. Moreau, F. Nicoud, T. Poinsot, *Comptes Rendus Mécanique* 341 (2013) 131–140.

[105] A. Mishra, D.J. Bodony, *J. Sound Vibr.* 332 (2013) 821–838.
[106] P.A. Hield, M.J. Brear, *AIAA J.* 46 (2008) 517–527.
[107] A.F. Seybert, D.F. Ross, *J. Acoust. Soc. Am.* 61 (1977) 1362–1370.
[108] L. Crocco, W.A. Sirignano, Behavior of supercritical nozzles under three-dimensional oscillatory conditions. No. Agard-Ograph-117. Advisory Group for Aerospace Research and Development Neuilly-Sur-Seine (France), 1967.
[109] A.S. Morgans, C.S. Goh, J.A. Dahan, *J. Fluid Mech.* 733 (2013) R2.
[110] N. Karimi, M.J. Brear, W.H. Moase, *J. Fluid Mech.* 597 (2008) 67–89.
[111] S.R. Stow, A.P. Dowling, Thermoacoustic oscillations in an annular combustor, in: Proc. ASME Turbo Expo 2001, New Orleans, Louisiana, USA.
[112] W. Eversman, Theoretical models for duct acoustic propagation and radiation, in: Aeroacoustics of Flight Vehicles: Theory and Practice, vol. 2: Noise Control, (1991) 101–163.
[113] J.M. Tyler, T.G. Sofrin, Axial Flow Compressor Noise Studies, No. 620532. SAE Technical Paper, 1962.
[114] A.P. Dowling, *J. Fluid Mech.* 346 (1997) 271–290.
[115] A.P. Dowling, *J. Fluid Mech.* 394 (1999) 51–72.
[116] A.P. Dowling, *J. Sound Vib.* 180 (1995) 557–581.
[117] M.J. Zucrow, J.D. Hoffman*Gas Dynamics*, vol. 1, Wiley, New York, 1976.
[118] S.R. Stow, A.P. Dowling, *J. Eng. Gas Turbines Power* 131 (2009).
[119] S.R. Stow, A.P. Dowling, Low-order modelling of thermoacoustic limit cycles, in: Proc. of ASME Turbo Expo 2004.
[120] M. Freitag, J. Janicka, *Proc. Combust. Inst.* 31 (2007) 1477–1485.
[121] S. Roux, G. Lartigue, T. Poinsot, U. Meier, C. Berat, *Combust. Flame* 141 (2005) 40–54.
[122] R.A. Huls, A.X. Sengissen, P.J.M. Van der Hoogt, J.B.W. Kok, T. Poinsot, A. de Boer, *J. Sound Vibr.* 304 (2007) 224–229.
[123] P. Schmitt, B. Schuermans, K.P. Geigle, T. Poinsot, *J. Fluid Mech.* 570 (2007) 17–46.
[124] G. Staffelbach, L. Gicquel, G. Boudier, T. Poinsot, *Proc. Combust. Inst.* 32 (2009) 2909–2916.
[125] A. Schwarz, F. Flemming, M. Freitag, J. Janicka, *in: Combustion Noise*, Springer, Berlin, Heidelberg, 2009, pp. 63–88.
[126] R. Ewert, W. Schröder, *J. Comput. Phys.* 188 (2003) 365–398.
[127] R. Ewert, W. Schröder, *J. Sound Vibr.* 270 (2004) 509–524.
[128] F. Flemming, C. Olbricht, B. Wegner, et al., *Flow Turbul. Combust.* 75 (2005) 3–27.
[129] E. Gröschel, W. Schröder, P. Renze, M. Meinke, P. Comte, *Comput. Fluids* 37 (2008) 414–426.
[130] F. Flemming, M. Freitag, A. Sadiki, J. Janicka, Time resolved combustion noise investigation based on a wave equation approach, in: 12th AIAA/CEAS Aeroacoustics Conference, AIAA 26152006, Cambridge, MA, USA, 2006.
[131] C. Olbricht, F. Flemming, A. Sadiki et al., A study of noise generation by turbulent flow instabilities in a gas turbine model combustor, in: ASME Turbo Expo 2005: GT2005-69029, Reno-Tahoe, Nevada, USA.